Numerical simulation of multi-modal reflection in large acoustic waveguides with different terminations

Abdelbasset Harrachi, Christian Prax, David Marx, Florent Margnat

ENSTA Paristech Institut Pprime

Internship final report
M2-AE
Acoustical Engineering Master

Numerical simulation of multi-modal reflection in large acoustic waveguides with different terminations

---

By :
Mr. Abdelbasset Harrachi

Supervisors :
Dr. Cristian PRAX
Dr. David MARX
Dr. Florent MARGNAT

September 20, 2018

Abstract

Using microphone pairs is a standard method to measure the acoustic properties of a waveguide such as the reflection coefficient at the outlet. This method is used in many experimental works before and discussed in many scientific papers. In this study, the measurement of the reflection coefficient with microphone pairs method is simulated using a numerical model that represent exactly the experimental protocol in order to provide numerical results and support the experimental measurements.

The plane mode reflection in waveguides is largely described in literature, and many theoretical models are developed in this particular case which could be used to validate the experimental results, however the multi-modal reflection coefficient is more complicated to derive theoretically. Therefore, this study aims to provide a basis of comparison for the experimental measurements especially for the Multi-modal reflection coefficient of higher modes. The simulations are covering open-end pipes with three different termination geometries: a pipe ended with an infinite baffle, a pipe ended with a finite flange and a pipe ended with sharp edge (unbaffled).

The simulations are performed through the four major steps of a standard simulation: Pre-processing, sensitivity calculations and benchmark tests, computation and finally post-processing. In the end the numerical results are compared to experimental measurements conducted by Zhiping QIU [1] during his PhD study.

Résumé

Les mesures acoustiques par antennerie microphonique est devenue une méthode standard pour la détermination des propriétés acoustiques des guides d'ondes comme le coefficient de réflexion à l'extrémité du guide. Cette méthode est traitée dans plusieurs travaux expérimentaux et par plusieurs papiers scientifiques. Dans le cadre de ce stage, cette méthode est simulée par un model numérique qui reproduit exactement son protocole expérimental afin d'appuyer les mesures expérimentales par des résultats numériques.

La réflexion du mode plan est décrite dans plusieurs études théoriques, et cela donne une référence pour les mesures expérimentales. Par contre le développement d'un modèle théorique pour le coefficient de réflexion des modes supérieurs est plus compliqué d'où le but de notre étude est de fournir une base de comparaison pour les mesures du coefficients de réflexion des modes supérieurs en utilisant un modèle numérique. Les simulations dans cette étude couvrent trois types d'extrémités de guide d'ondes : guide avec un plan infini à l'extrémité, guide avec une bride à l'extrémité et un guide avec une extrémité sans épaisseur.

Les simulations sont partagées en quatre grandes étapes : le prétraitement, calculs de sensibilités, lancement des calculs et finalement le post traitement. A la fin les résultats numériques sont comparés avec les mesures effectuées par Zhiping QIU [1] durant son PhD.

...

Acknowledgments

I would like to thank *Dr. Yves GERVAIS* head of *Institut Pprime* laboratory and all those who participated and helped me to have such an enjoyable and beneficial experience. Furthermore, I would like to express my deepest appreciation to the expert insight and crucial role of *Dr. David MARX* in this internship, who provided me all the necessary information, materials and time to help me understand and solve all the problems encountered during this project. I would also like to acknowledge with much appreciation *Dr. Florent MARGNAT* and *Dr. Cristian PRAX* for their guidance and their help with the simulations and the validation of the numerical modal. A special thanks go to *Dr. Hélène BAILLIET*, *Dr. Jean-Christophe VALIERE* and *Dr. Zhiping QIU* who provided the necessary data of their experimental work and for their practical perspective and comments that guided me throughout this internship. Last but not least, I have to mention that I spent this internship in the best possible conditions thanks to *Jean-Christophe VERGEZ* for his IT interventions and *Bouba EL HARCHI* for her help with the administrative work.

Contents

I Introduction:

I.1 Motivation:

Acoustic waveguides are used in many industrial applications from aeronautics to music industry, and in general waveguides are open end ducts because in real life waveguides are finite and infinite ducts are just an idealization for theoretical purposes. The acoustic propagation in infinite waveguides is relatively fully described in literature, however for open waveguides it is more complicated to derive theoretical equations that describe what occurs at the open end. Because of the sudden change of the geometry at the open-end of the finite waveguide and under the action of the surrounding fluid, the acoustic impedance at the outlet of the pipe is different from the impedance inside the pipe which leads to a reflection phenomenon. This phenomenon becomes more complicated in multimodal propagation case, which is the case in the most industrial applications.
Actually, the reflection occurs outside the waveguide at a small distance δ from the exit [3]. This distance is called the *length correction* or *end correction* because it should be taken into account as an additional length to the physical length of the duct (geometric length). The acoustic characteristics of the waveguide such as resonance frequencies are impacted by this length correction. For example the calculation of resonance frequencies of an open pipe of length L is more accurate if performed with a length of $L + \delta$ thus $f_r = \frac{(2n+1)c_0}{4(L+\delta)}$ instead of $f_r = \frac{(2n+1)c_0}{4L}$.
Therefore a good understanding of this phenomenon is required in order to improve the design of the systems used in everyday life like aircraft jet engines, exhaust mufflers, music instruments...

In jet engines:

The acoustic instabilities could lead to combustion instabilities in the combustion chamber, therefore the acoustic behaviour should be known at the inlet and the outlet of the engine that could be considered as a large waveguide.

In ventilation duct:

One of the most important factors to take into account in the design of ventilation ducts is noise control. The noise of the ventilation system should be as quiet as possible, especially in quiet confined places like offices, because being exposed to a constant noise created by ventilation fans for an extended period of time could negatively impact our health.

In music instruments:

Acoustic wave propagation in waveguides is largely used in the music industry, for example in the design of music instruments like the flute and the trumpet where a shift of a couple hertz in the sound frequency makes a big difference in the sound quality of the instrument.

I.2 Objectives:

The main goal of this study is the calculation of the multimodal reflection coefficient using numerical simulations in order to support the experimental results found by Zhiping QIU during his PhD [1]. Using an experimental approach, Zhiping gives the multimodal reflection coefficients and the multimodal correction length in open end circular ducts. He also considers 3 different pipe exits: baffled pipe, flanged pipe and unbaffled pipe. The experimental results for the plane wave are in good agreement with the theoritical expressions given by Norris and

Sheng [6], however for higher modes we need to provide some numerical results in order to verify the accuracy of the measurements.
Zhiping's results are summarized in figure 1 and figure 2:

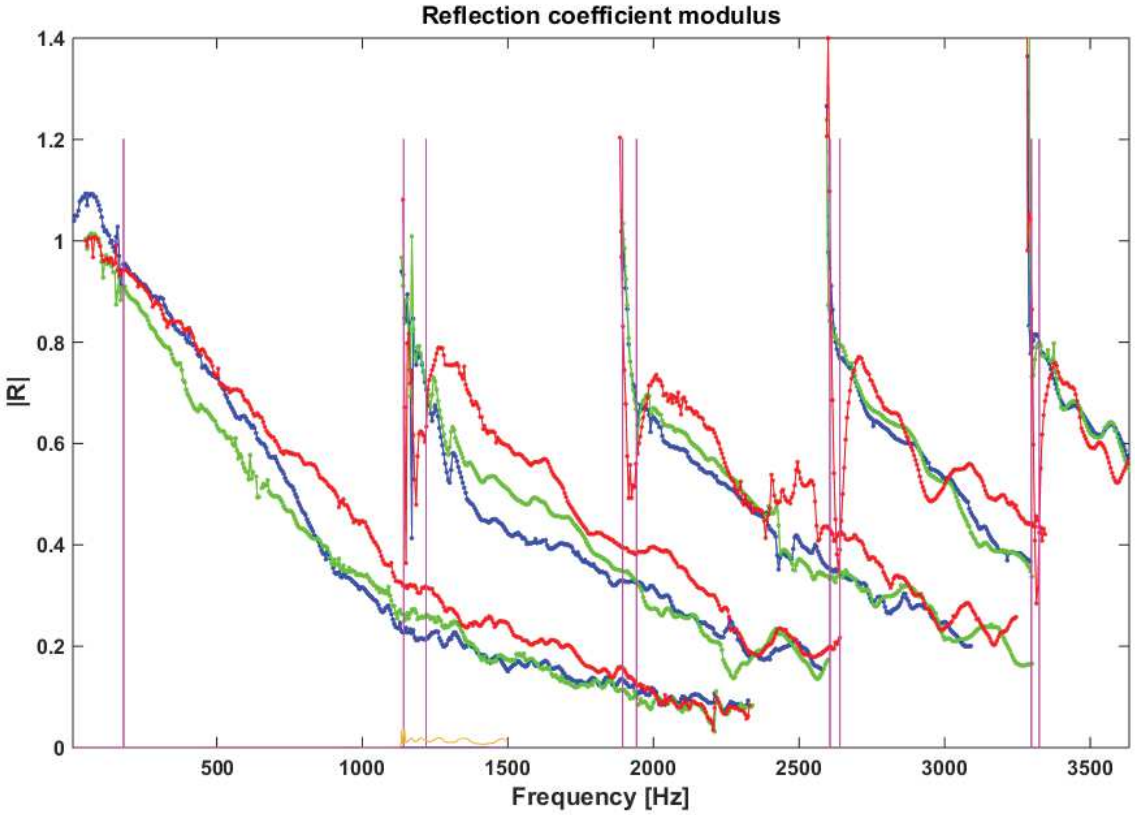

Figure 1 – Experimental results of multimodal reflection coefficients modulus: red curves correspond to the unbaffled pipe, green curves correspond to the baffled pipe and the blue ones correspond to the flanged pipe. The vertical bars marks the regions where the measurements are more sensitive to noise.

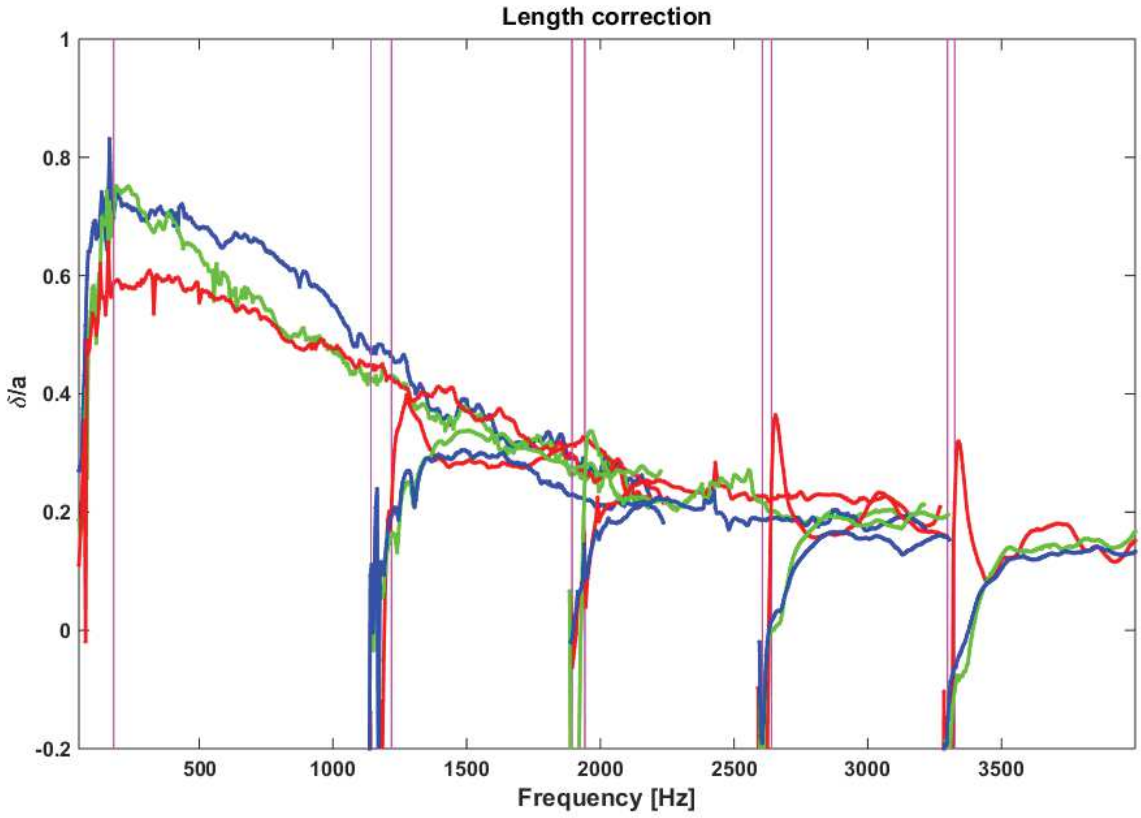

Figure 2 – Experimental results of multimodal length correction: red curves correspond to the unbaffled pipe, green curves correspond to the baffled pipe and the blue ones correspond to the flanged pipe. "a" is the radius of the pipe. The vertical bars marks the regions where the measurements are more sensitive to noise.

II Background on multimodal propagation in waveguides:

II.1 Multimodal propagation in circular ducts:

With linear acoustics assumptions, the acoustic waves propagation is governed by Helmholtz equation:

$$\frac{\partial^2 p}{\partial t^2} - c_0^2 \Delta p = 0 \tag{1}$$

Where p and c_0 are respectively the pressure fluctuation and sound speed. Using separation of variables method in cylindrical coordinates, the solutions of Helmholtz equation in circular duct and in a harmonic regime of pulsation $\omega = 2\pi f$ (f is the frequency) have the following form [2]:

$$p(r,\theta,z,t) = \underbrace{\psi(r,\theta)}_{transverse} \underbrace{[P^+ e^{-i\gamma z} + P^- e^{i\gamma z}]}_{axial} e^{i\omega t} \tag{2}$$

Where (r,θ,z) are the cylindrical coordinates, γ is the axial component of the wavenumber and (P^+,P^-) are the pressure wave amplitudes of waves traveling respectively toward $+z$ and $-z$. In cylindrical coordinates the Laplacian operator is:

$$\Delta = \frac{\partial^2}{\partial r^2} + \frac{1}{r^2}\frac{\partial}{\partial r} + \frac{1}{r^2}\frac{\partial^2}{\partial \theta^2} + \frac{\partial^2}{\partial z^2} = \Delta_{r\theta} + \frac{\partial^2}{\partial z^2} \tag{3}$$

Where $\Delta_{r\theta}$ is the Laplacian in the section of the pipe. From equations 1 and 2 the wave equation becomes:

$$\Delta_{r\theta}\psi + \underbrace{[k^2 - \gamma^2]}_{k_{r\theta}^2}\psi = 0 \tag{4}$$

Where $k = \frac{\omega}{c_0}$ is the total wavenumber and $k_{r\theta}$ is the transverse wavenumber. Using separation of variables, the in-plane pressure field function ψ can be written as $\psi(r,\theta) = f(r)g(\theta)$ and in this case equation 4 becomes:

$$\frac{r^2}{f}(\frac{\partial^2}{\partial r^2} + \frac{1}{r}\frac{\partial}{\partial r})f + k_{r\theta}^2 r^2 = -\frac{1}{g}\frac{\partial^2 g}{\partial \theta^2} \tag{5}$$

The left side of the equation 5 depends on r and the right side depends on θ then both sides are constant:

$$\frac{r^2}{f}(\frac{\partial^2}{\partial r^2} + \frac{1}{r}\frac{\partial}{\partial r})f + k_{r\theta}^2 r^2 = -\frac{1}{g}\frac{\partial^2 g}{\partial \theta^2} = m^2 \tag{6}$$

then:

$$\frac{\partial^2 g}{\partial \theta^2} + m^2 g = 0 \tag{7}$$

$$r^2(\frac{\partial^2}{\partial r^2} + \frac{1}{r}\frac{\partial}{\partial r})f + [k_{r\theta}^2 r^2 - m^2]f = 0 \tag{8}$$

The general solution of equation 7 is:

$$g_m(\theta) = Ae^{im\theta} + Be^{-im\theta} \ (m \in \mathbb{N}) \tag{9}$$

or

$$g_m(\theta) = A_m e^{im\theta} \ (m \in \mathbb{Z}) \tag{10}$$

By introducing the variable $\xi = k_{r\theta} r$ in equation 8 we obtain the following equation:

$$\xi^2(\frac{\partial^2}{\partial \xi^2} + \frac{1}{\xi}\frac{\partial}{\partial \xi})f + [\xi^2 - m^2]f = 0 \tag{11}$$

The general solutions of the equation 11 are Bessel functions (J_m) of the first kind and the m^{th} order.
The rigid wall boundary condition on the pipe $r = a$ (a is the radius of the pipe) can be written as:

$$V_n = \frac{\partial p}{\partial n} = \frac{\partial p}{\partial r} = 0 \ \ (for\ r = a)$$

Then

$$\frac{\partial f}{\partial r} = \frac{\partial J_m(\xi)}{\partial r} = J'_m(\xi) = 0 \ \ (for\ r = a \iff \xi = ak_{r\theta})$$

So ξ corresponds to α_{mn} the roots of the first derivative of Bessel function J_m of the first kind, then $\xi_{mn} = \alpha_{mn}$ where (m) is the order of the Bessel function and (n) is the rank of the root. Then the function f can be written as:

$$f(r) = J_m(\frac{\alpha_{mn}}{a}r) \tag{12}$$

The following table gives the first roots of the first derivative of Bessel function of the first kind:

α_{mn}	n=0	n=1	n=2
m=0	0.0	3.831	7.015
m=1	1.841	5.331	8.536
m=2	3.054	6.706	9.969

Finally the transverse pressure field $\psi_{mn}(r, \theta)$ has the following form:

$$\psi_{mn}(r, \theta) = f(r)g(\theta) = A_{mn}e^{im\theta}J_m(\frac{\alpha_{mn}}{a}r) \ (m \in \mathbb{Z}) \tag{13}$$

According to the general form of the transverse pressure field ψ_{mn}, the transverse pressure is composed of modes (m, n). Knowing that $\xi_{mn} = ak^{mn}_{r\theta}$ and $k^2 = \gamma^2_{mn} + (k^{mn}_{r\theta})^2$ then we can express the axial wavenumber as following:

$$\gamma_{mn} = \sqrt{k^2 - (\frac{\alpha_{mn}}{a})^2} \tag{14}$$

γ_{mn} is null at $f = f^{mn}_c$ where f^{mn}_c is called the cutoff frequency of the mode (mn):

$$f^{mn}_c = \frac{\alpha_{mn}c_0}{2a\pi} \tag{15}$$

Depending on the value of $k = \frac{2\pi f}{c_0}$ (the frequency), γ_{mn} could be an *imaginary* or a *real* number. If $f > f^{mn}_c$ γ_{mn} is real and the mode (mn) propagates, contrary if $f < f^{mn}_c$ the mode can not propagate and its pressure amplitude decreases exponentially in the pipe, it is called an *evanescent mode*.

Finally the pressure field in the pipe is a combination of the axial and the transverse fields of each mode (mn), then the total pressure field is the infinite sum of these modes:

$$p(r, \theta, z, \omega) = \sum_{m=-\infty}^{+\infty}\sum_{n=0}^{+\infty}[P^+_{mn}e^{-i\gamma_{mn}z} + P^-_{mn}e^{i\gamma_{mn}z}]J_m(\frac{\alpha_{mn}}{a}r)e^{i(m\theta+\omega t)} \tag{16}$$

II.2 Reflection coefficient and length correction:

II.2.1 Reflection of a plane mode ($mn = 00$):

At the open end of a rigid pipe, the impedance Z imposed by the surrounding fluid (air) sends back a part of the incoming wave in the opposite direction. Thus a wave traveling along a rigid open end duct is a superposition of two waves, the incoming wave and the reflected wave. And of course the reflection coefficient is directly related to the impedance Z.
For simplification purposes we consider in our theoretical derivation only plane waves (mode 00) propagation in infinitely baffled and rigid pipe.

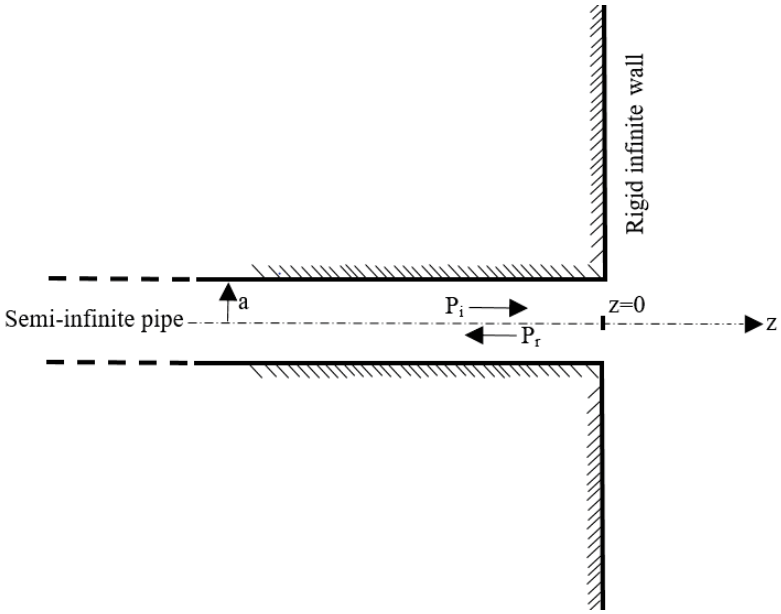

Figure 3 – Geometry and parameters of the problem

One can consider a rigid semi infinite pipe baffled with an infinite rigid wall at the outlet as depicted in figure 3. In this configuration the pressure wave in the duct is the sum of the incoming P_i and the reflected P_r wave:

$$P = P_i + P_r$$

According to the calculations in paragraph II.1 and with the assumption of the plane wave propagation in the harmonic regime, the pressure fields in the pipe are:

$$P_i = P^+ e^{-ikz} \text{ and } P_r = P^- e^{ikz}$$

Where P^+ and P^- are respectively the incoming and reflected waves amplitudes, $k = \frac{\omega}{c_0} = \gamma_{00}$ is the wave number, ω is the pulsation of the wave and c_0 is the sound speed. By definition the reflection coefficient is [3]:

$$R = \frac{P^-}{P^+} \tag{17}$$

thus:

$$P = P^+[e^{ikz} + R\, e^{-ikz}] \tag{18}$$

Using Euler equation $\rho \frac{\partial V}{\partial t} = -\nabla P$ the velocity field is:

$$V = \frac{P^+}{\rho c}[e^{ikz} - R\, e^{-ikz}] \tag{19}$$

Where ρ is the mass density of the fluid (air).
The impedance at the outlet of the pipe ($z = 0$) is $Z = \frac{P(z=0)\Sigma}{V(z=0)}$, where $\Sigma = \pi a^2$ is the area of the pipe cross section. From equations 18 and 19 we get the following expression:

$$Z = \rho c \frac{1+R}{1-R}\Sigma \tag{20}$$

The equation 20 shows the relationship between the reflection coefficient and the impedance at the outlet of the duct, in this case we can deduce the reflection coefficient by measuring, simulating or calculating theoretically the impedance Z.

For the plane mode, the velocity is the same in each point of a given cross section of the pipe, so one can consider the section at the outlet of the pipe ($z = 0$) as a vibrating baffled piston at a constant velocity amplitude V_p. Rayleigh integral gives the pressure at an observer location $\vec{r}$ outside the pipe by:

$$P(r) = -\frac{2i\,k\,\rho\,c}{4\pi} V_p \iint_\Sigma \frac{e^{ik\acute{r}}}{\acute{r}} d\sigma \tag{21}$$

Where $\acute{r}$ is the distance between the observer location and the integration point on the piston. Knowing the pressure field, one can calculate the force applied on the piston by: $F = \iint_\Sigma P(\sigma) d\sigma$ which means that F is a quadruple integral over the pipe cross section. So the impedance expression is:

$$Z = \frac{F}{V_p} = -\frac{2i\,k\,\rho\,c}{4\pi} \iiiint_\Sigma \frac{e^{ik\acute{r}}}{\acute{r}} d\sigma \tag{22}$$

The calculation of this integral is done by Rayleigh (1896) [4] and Pierce (1989) [5], and the final expression of the impedance at the outlet of the pipe is:

$$Z = \rho\,c\,\pi\,a^2[1 - \frac{J_1(2ka)}{ka} - i\frac{S_1(2ka)}{ka}] \tag{23}$$

Where J_1 and S_1 are respectively Bessel and Struve functions of the first kind. In low frequency range ($ka << 1$) Bessel and Struve functions could be approximated by: $1 - \frac{J_1(2ka)}{ka} = \frac{(ka)^2}{2}$ and $\frac{S_1(2ka)}{ka} = \frac{8ka}{3\pi}$. The real part of the impedance Z represent the radiated part of the wave and the imaginary part of Z is equivalent to a vibrating mass:

$$Im(Z) = -\rho a^2 \pi \underbrace{\left(\frac{8a}{3\pi}\right)}_{\delta \simeq 0.85a} \omega \tag{24}$$

Actually the reflection phenomenon occurs outside the pipe at a small distance δ from the open end [3]. The moving mass is equivalent to a cylinder with the same cross section as the pipe and a height of $\delta \simeq 0.85a$, thus the reflection phenomenon occurs at a point located at a distance δ outside the pipe, δ is called "*length correction*".

More elaborated calculation, done by Norris and Sheng [6] gives an approximation of the reflection coefficient and the length correction for $ka < 3.8$:

$$|R| = \frac{1 + 0.323ka - 0.077(ka)^2}{1 + 0.323ka + (1 - 0.077)(ka)^2} \tag{25}$$

$$\delta = a\frac{0.82159 - 0.49(ka)^2}{1 - 0.46(ka)^3}$$

We can verify that the expression of Norris and Sheng gives a length correction of $\delta(ka = 0) \simeq 0.82a$ which is close to the value $0.85a$ given by Rayleigh [4]. The results of the expressions given by Norris and Sheng are summarized in figure 4:

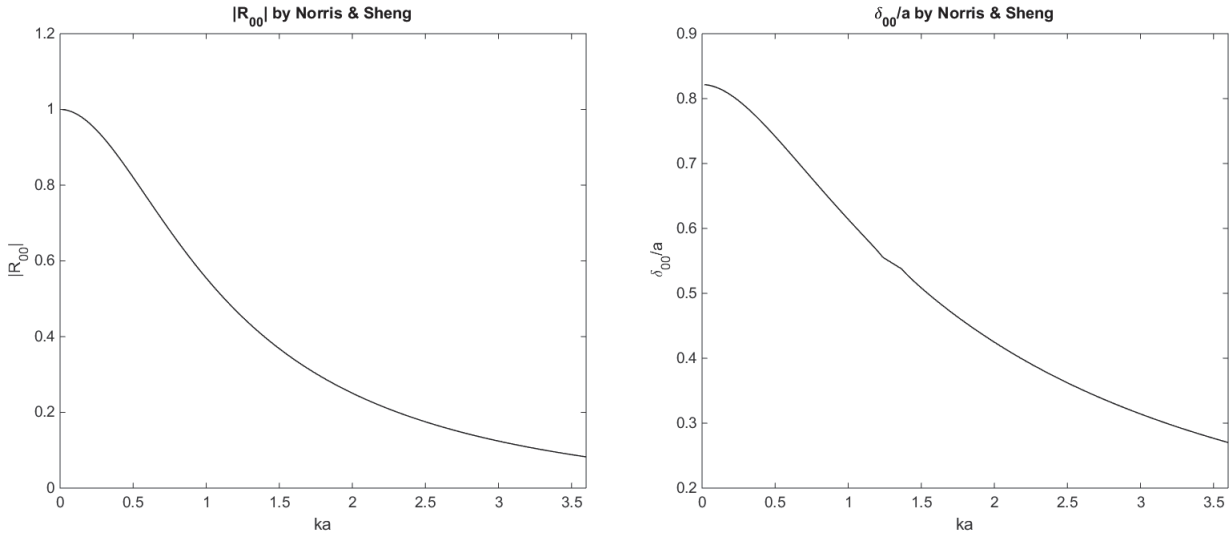

Figure 4 – Reflection coefficient magnitude and length correction according to Norris and Sheng expressions

II.2.2 Reflection of higher modes:

The reflection coefficient is defined as the ratio of the pressure amplitude of the wave traveling toward $-z$ and the one traveling toward $+z$ (P^- and P^+). These amplitudes depend on the propagating mode in the pipe, which means that the reflection coefficient depends also on the mode [3]:

$$R_{mn} = \frac{P^-_{mn}}{P^+_{mn}} \tag{26}$$

The multimodal length correction δ_{mn} is directly related to the phase of the reflection coefficient R_{mn} [3]:

$$R_{mn}(z=0) = -|R_{mn}|e^{-2i\gamma_{mn}\delta_{mn}} \tag{27}$$

Where $z = 0$ is the coordinate of the open end. The calculation of the multimodal reflection coefficient is derived in the next paragraph.

II.2.3 Modal decomposition of the pressure field in circular ducts:

II.2.3.1 Calculation of the reflection coefficient R_{m0} for the azimuthal modes:

As shown in the previous section, a mode could propagates in the pipe if the frequency of excitation is higher than its cutoff frequency. Therefore the modes appear in the same order of their cutoff frequencies, provided that the boundary conditions allow their propagation. Then all the modes of a cutoff frequency lower than the frequency of excitation could propagate freely in the pipe, which means that in general the pressure field is a mixture of many propagating modes as depicted in figure 5.

In this section we discuss the calculation of the reflection coefficient R_{mn}, using the total pressure amplitude of the mode $P_{mn} = P^+_{mn}(\omega, z) + P^-_{mn}(\omega, z)$. For simplification purposes, we consider only the first azimuthal modes ($m0$).

Let's consider two different positions on the pipe axis (z_0,z_1) where the pressure amplitudes of the mode ($m0$) are [2]:

$$\begin{aligned} P_{m0}(\omega, z_0) &= P^+_{m0}(\omega)e^{-i\gamma_{m0}z_0} + P^-_{m0}(\omega)e^{i\gamma_{m0}z_0} \\ P_{m0}(\omega, z_1) &= P^+_{m0}(\omega)e^{-i\gamma_{m0}z_1} + P^-_{m0}(\omega)e^{i\gamma_{m0}z_1} \end{aligned} \tag{28}$$

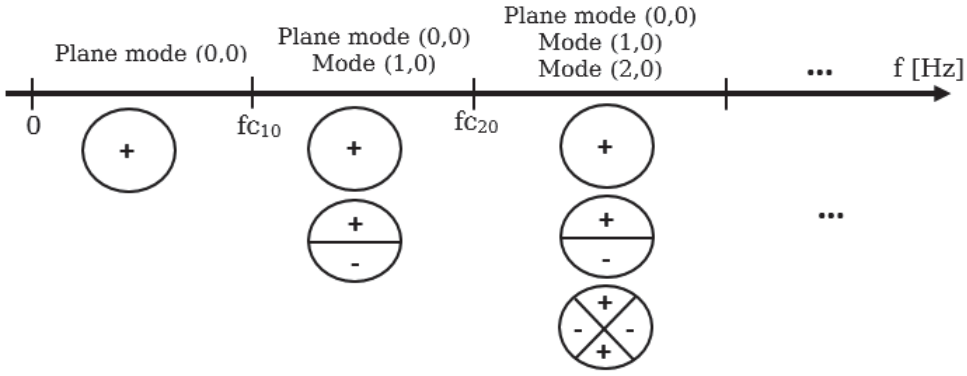

Figure 5 – Order of appearance of the modes in circular waveguides

The unknowns $P^+_{m0}(\omega)$ and $P^-_{m0}(\omega)$ could be calculated from this system of equations if the two equations are independent, which means that the *determinant* of the matrix system is not nil [7]:

$$\begin{aligned} \det \begin{vmatrix} e^{-i\gamma_{m0}z_0} & e^{i\gamma_{m0}z_0} \\ e^{-i\gamma_{m0}z_1} & e^{i\gamma_{m0}z_1} \end{vmatrix} &\neq 0 \\ \Rightarrow s = z_1 - z_0 \neq \frac{n\pi}{\gamma_{m0}};\ (n \in \mathbb{N}) & \end{aligned} \tag{29}$$

For the following calculations, we assume that the modal pressure amplitude P_{m0} is measured or calculated at positions (z_0,z_1) that fulfill the condition (29).

We can take $z_0 = 0$ and $z_1 = s$, then the previous system of equations becomes:

$$P_{m0}(\omega, 0) = P^+_{m0}(\omega) + P^-_{m0}(\omega) \tag{30}$$

$$P_{m0}(\omega, s) = P^+_{m0}(\omega)e^{-i\gamma_{m0}s} + P^-_{m0}(\omega)e^{i\gamma_{m0}s}$$

Thus the amplitudes of the outgoing wave and the reflected one are:

$$\begin{aligned} P^-_{m0}(\omega) &= \frac{P_{m0}(\omega, 0)e^{-i\gamma_{m0}s} - P_{m0}(\omega, s)}{e^{-i\gamma_{m0}s} - e^{i\gamma_{m0}s}} \\ P^+_{m0}(\omega) &= \frac{P_{m0}(\omega, s) - P_{m0}(\omega, 0)e^{i\gamma_{m0}s}}{e^{-i\gamma_{m0}s} - e^{i\gamma_{m0}s}} \end{aligned} \tag{31}$$

The reflection coefficient should be calculated at the outlet of the pipe at a given position on the axis $z = L$ ($L \neq s$), therefore the phase of the pressure amplitudes changes and become:

$$\begin{aligned} P^-_{m0}(\omega, L) &= \frac{P_{m0}(\omega, 0)e^{-i\gamma_{m0}s} - P_{m0}(\omega, s)}{e^{-i\gamma_{m0}s} - e^{i\gamma_{m0}s}} e^{i\gamma_{m0}L} \\ P^+_{m0}(\omega, L) &= \frac{P_{m0}(\omega, s) - P_{m0}(\omega, 0)e^{i\gamma_{m0}s}}{e^{-i\gamma_{m0}s} - e^{i\gamma_{m0}s}} e^{-i\gamma_{m0}L} \end{aligned} \tag{32}$$

Then the reflection coefficient at the outlet of the pipe is [8]:

$$R_{m0}(\omega, L) = \frac{P^-_{m0}(\omega, L)}{P^+_{m0}(\omega, L)} = \frac{P_{m0}(\omega, 0)e^{-i\gamma_{m0}s} - P_{m0}(\omega, s)}{P_{m0}(\omega, s) - P_{m0}(\omega, 0)e^{i\gamma_{m0}s}} e^{2i\gamma_{m0}L} \tag{33}$$

Finally if P_{m0} is known, R_{m0} could be deduced using the formula 33. In the next paragraph, the calculation of the modal pressure amplitudes P_{m0} using finite number of measurement points is presented.

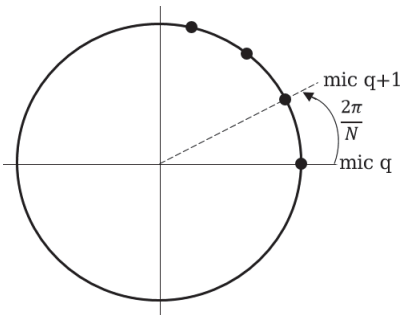

Figure 6 – Microphone positioning on the circumference of the pipe section

II.2.3.2 Decomposition of azimuthal modes P_{m0}:

According to the equation 16 the pressure field in the pipe depends on the position (r, θ, z) and the frequency:

$$p(r,\theta,z,\omega) = \sum_{m=-\infty}^{+\infty} \sum_{n=0}^{+\infty} P_{mn}(\omega,z) J_m(\frac{\alpha_{mn}}{a} r) e^{im\theta} \tag{34}$$

Using the same simplifications as before, we consider only azimuthal modes ($n = 0$):

$$p(r,\theta,z,\omega) = \sum_{m=-\infty}^{+\infty} P_{m0}(\omega,z) J_m(\frac{\alpha_{mn}}{a} r) e^{im\theta} \tag{35}$$

One can consider only the pressure on the circumference of the section where ($z = z_0$ and $r = a$ the radius of the pipe):

$$p(a,\theta,z_0,\omega) = \sum_{m=-\infty}^{+\infty} P_{m0}(\omega,z_0) e^{im\theta} \tag{36}$$

We can see that the pressure field on the circumference of the section is the *discrete Fourier transform* of the modal pressure amplitude P_{m0}, therefore P_{m0} could be calculated using the *inverse Fourier transform* of the pressure field on the circumference $p(a, \theta, \omega)$. In a real experiment (or a simulation), it would be more practical to measure (or calculate) the pressure field on a finite number of points on the circumference using microphones (or numerical probes). Let's consider N microphones (or numerical probes) placed on the circumference of the section with a uniform spacing between each two microphones of $\frac{2\pi}{N}$ as depicted in figure 6. In this case the discrete inverse Fourier transform of the measured pressure field is [9]:

$$P_{m0}(z_0,\omega) = \frac{1}{N} \sum_{q=0}^{N-1} p(a,\theta_q,z_0,\omega) e^{-2im\frac{q\pi}{N}} \tag{37}$$

In the following sections, equations 33 and 37 will be used to calculate the multi-modal reflection coefficient of the first azimuthal modes (0,0), (1,0) and (2,0) using numerical simulations.

III Numerical setup and methodology:

The main goal of this study is the calculation of the reflection coefficient and the length correction for open end waveguides using numerical simulations in order to support the experimental results found by Zhiping QIU [1] during his PhD. The software used is *Comsol Multiphysics*, a multi-physics simulation software which includes geometry building and meshing modules. A 3D model of the domain is build in Comsol environment considering the requirements described in the following paragraphs.

III.1 Preprocessing and preparation of the model:

III.1.1 Building the numerical model:

The simulation problem is defined by 4 major elements: the domain, the boundary conditions, the equation to solve (and the algorithm used) and finally the excitation.

The domain:

A rigid wave-guide with a circular cross section is considered. The radius and the length of the pipe are respectively a and l. At the outlet of the pipe the infinite space is represented with a half of sphere or a complete sphere, depending on the exit geometry. For a baffled exit we use a half of sphere however we use a complete sphere for the unbaffled and the flanged pipe. The radius of the sphere R should verify the far field condition, because the waves should impinge on the spherical surface at the far field where they could be considered as spherical waves. The minimum radius of the sphere is defined after a sensitivity analysis in section IV. The used fluid is air ($C = 340ms^{-1}$ and $\rho = 1.23kgm^{-3}$). Figure 7 shows the geometry of the studied domain.

The boundary conditions:

Three types of boundary conditions are used in the simulations: rigid wall, non-reflection condition and imposed acceleration. The rigid wall condition is used on the pipe walls and the baffle and the flange surfaces. Rigid wall boundary condition consists on forcing the normal velocity of the fluid to zero ($\vec{V}.\vec{n} = V_n = 0$) where $\vec{n}$ is the normal to the surface. Otherwise, and using Euler equation, this condition could be rewritten as: $\nabla P.\vec{n} = 0$. The second boundary condition is the non-reflection condition, this condition is used on the spherical surface in order to model the boundary between the modeled domain and the infinite domain. This condition minimizes the reflections when the waves leave the modeling domain. According to *Comsol User's Guid* [11] after Bayliss, Gunzburger and Turkel [12] the expression of non-reflection boundary condition in spherical geometry is:

$$-\vec{n}.(-\frac{1}{\rho}\nabla p) + (i\ k + \frac{1}{r})\frac{p}{\rho} = (i\ k + \frac{1}{r})\frac{p_i}{\rho} + \vec{n}.(\frac{\nabla p_i}{\rho}) \tag{38}$$

Where p_i is the incoming pressure wave.
The last type of boundary conditions used in the simulations is the imposed acceleration. This condition is used to model the vibration of the loudspeaker, and the expression of this condition is given by Euler equation: $\rho\dot{V} = \rho\frac{\partial V}{\partial t} = -\nabla P$.

The excitation:

In the simulations, the loudspeakers are modeled with a small vibrating portion of the pipe wall at the bottom of the model, in the same configuration used by Q.Zhiping [1] in his experiment.

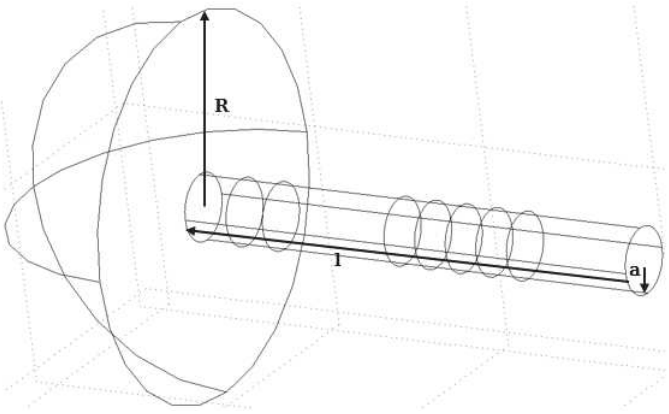

(a) Geometry used for the baffled pipe

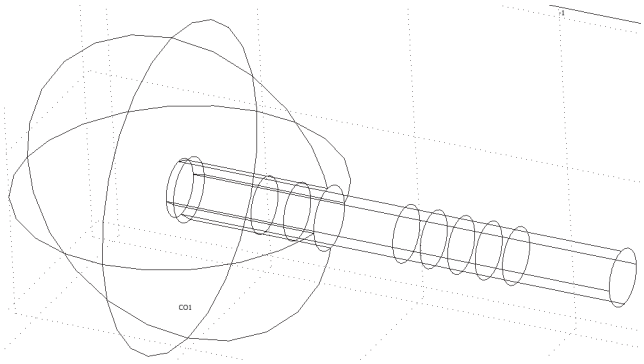

(b) Geometry used for the flanged and unbaffled pipe

Figure 7 – Geometry of the domain

Figure 8 shows all the boundary conditions used in our simulations.

To simulate a semi-infinite pipe the boundary condition on the bottom of the pipe should be a non-reflection condition, but in the simulations we use a rigid wall condition in order to keep the same configuration used in the test bench of Q.Zhiping [1].

The dimensions of the model will be presented in section IV.

III.1.2 Solving Helmholtz equation using BiCGSTAB algorithm:

The problem is studied in the time-harmonic regime under linear acoustic assumptions, thus the equation used is Helmholtz wave equation [11]:

$$\nabla[\frac{1}{\rho}\nabla p] + \frac{k^2}{\rho}p = 0 \tag{39}$$

The algorithm used to solve the matrix problem based on this equation is the Biconjugate Gradient Stabilized algorithm "$BiCGSTAB$". This algorithm is used to solve a linear algebra problem $A\ x = b$ without any symetry conditions on the matrix A, the algorithm proceeds as following [10]:

- Give an arbitrary initial value to the vector $x = x_0$;
- Calculate $r_0 = b - A\ x_0$;
- Choose an arbitrary vector $\hat{r}_0$ such that $\hat{r}_0$ and r_0 are not orthogonal;

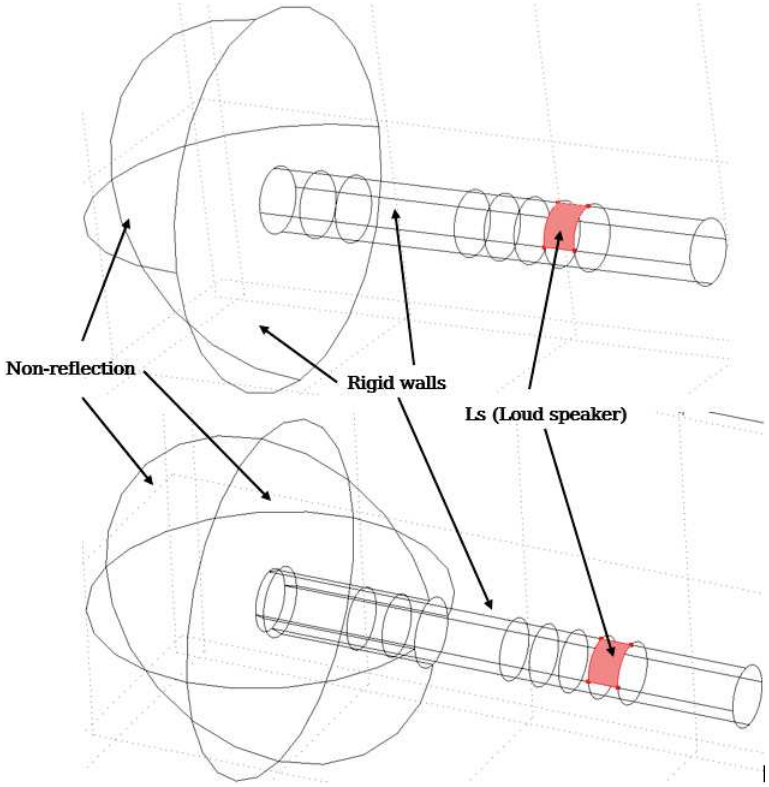

Figure 8 – Boundary conditions used in the simulations

- start a loop i=0,1,2,...:
  - $\alpha_i =< \hat{r}_0, r_i > / < Ap_i, \hat{r}_0 >$ where $< ., . >$ is the scalar product;
  - $s_i = r_i - \alpha_i A p_i$;
  - $\omega_i =< As_i, s_i > / < As_i, As_i >$;
  - $x_{i+1} = x_i + \alpha_i p_i + \omega_i s_i$;
  - $r_{i+1} = s_i - \omega_i A s_i$;
  - if $||r_{i+1}|| < \epsilon_0$, break the loop. Where ϵ_0 is the maximum accepted error (threshold);
  - $\beta_i = (\alpha_i/\omega_i) < r_{i+1}, \hat{r}_0 > / < r_i, \hat{r}_0 >$;
  - $p_{i+1} = r_{i+1} + \beta_i(p_i - \omega_i A p_i)$;
- set $x = x_{i+1}$;

III.2 Modal decomposition and Post-processing:

Comsol includes a post-processing module that allow to plot the acoustic pressure and velocity fields which is very useful to verify some details in the model like the boundary conditions by analyzing the global behavior of the waves. However this module shows the total pressure field and it could not extract the modes, the reason why we used a *Matlab* code for the modal extraction.

III.2.1 Modal decomposition code:

It is possible to export the pressure field data from Comsol model using *Export Postprocessing data* on a finite number of points in the model (*probes*). These probes represent the microphones in the experiment of Q.Zhiping [1]. We kept the same number of microphones used

in the experiment ($N = 8$ microphones) placed with a $\frac{\pi}{4}$ angular gap between each couple of microphones as described in section II.2.3.2.

In our model, the microphones are defined as a group of 3 probes with a gap of $\pm 2deg$ between each two probes as depicted in figure 9 and the pressure on the the microphone is the average of the pressure calculated on these 3 probes.

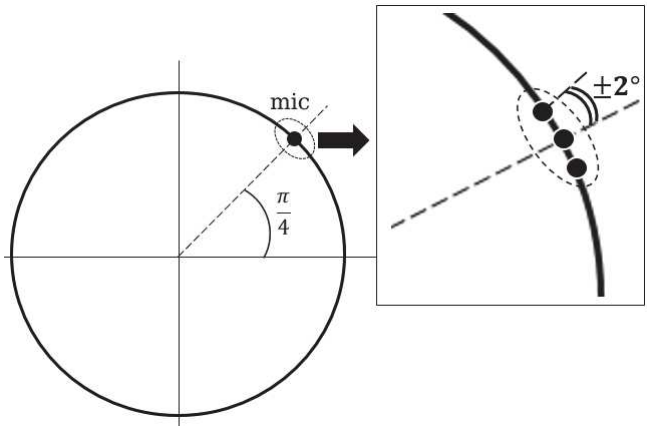

Figure 9 – Modeling a microphone with a 3 points probe

We used two measurement sections as shown in figure 10, the same number of sections used by Q.Zhiping [1], and since we used 8 microphones on each section and each microphone is represented with 3 probes we have 48 probes in the model. Using the coordinates of the probes, we could generate a *postprocessing data file* containing the complex pressure calculated on the given points for all the simulated frequencies.

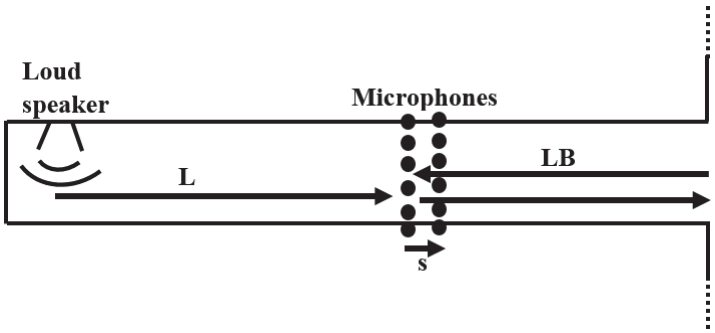

Figure 10 – Measurment sections used in the modal extraction ($s = 40mm$)

A Matlab code was created to extract the modes from the pressure data. The code contain 3 main parts:

- "*Read txt*" is the program used to read the data file generated by Comsol;
- "*Modal extract*" is the main program, used for the modal extraction;
- "*Plot curve*" is the program used for the post processing and results comparison.

Read txt:

The program *Read txt* reads the pressure data file and generates a matrix of complex pressure for each measurement section, the number of lines of each matrix corresponds to the number of microphones on each section and the number of columns corresponds to the number of the simulated frequencies:

Section i	f_1	f_2	...	f_{n-1}	f_n
mic_1	p_{11}	p_{12}	...	$p_{1\,n-1}$	$p_{1\,n}$
mic_2	p_{21}	p_{22}	...	$p_{2\,n-1}$	$p_{2\,n}$
...	...	...	...	...	...
...	...	...	...	...	...
mic_8	p_{81}	p_{82}	...	$p_{8\,n-1}$	$p_{8\,n}$

This program generates also the frequency vector used in the simulation and the coordinates of the microphones.

Modal Extract:

The program *Modal Extract* imports the matrices generated by *Read txt* (pressure, frequency and coordinates) and calculates the inverse Fourier transform using the expression in equation 37 and the parameters of the numerical model. In the end the reflection coefficient and the length correction are calculated using equation 33 and 27.

Plot curve:

This Program import the matrices generated by *Modal Extract* (R_{m0}, δ_{m0}, frequency, cutoff frequencies) in order to plot the results.

Figure 11 summarizes the process of post-processing described above:

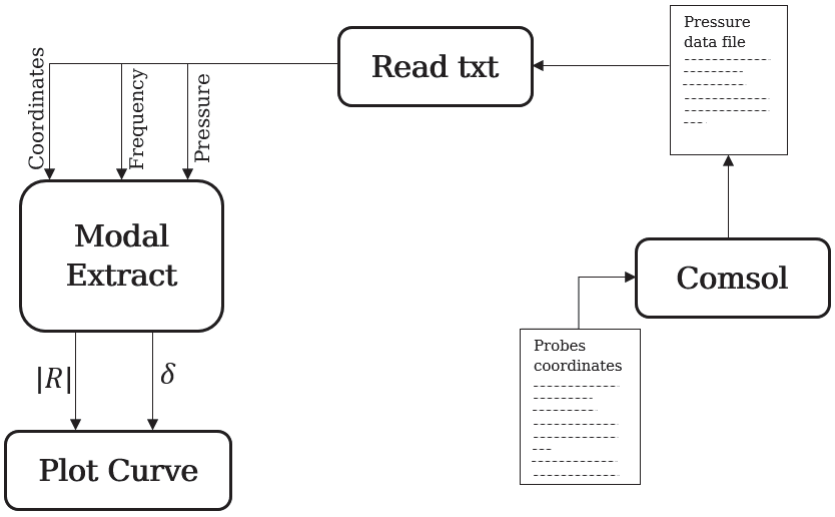

Figure 11 – Post-processing diagram

III.2.2 Benchmark tests of the post-processing code:

After building and debugging the programs described above, some benchmark tests have been performed in order to verify that the programs give the expected results, especially the modal extraction program.

III.2.2.1 Synthetic signal test:

In this test a new Matlab code called "*Pressure signal test*" is built in order to simulate "artificial" pressure signals of the microphones and use these signals in the main program "Modal Extract" to verify if the results correspond to the input data. Since the pressure signal is fully controlled in this case, we can control the reflection coefficient and the length correction, and we can compare the results of the modal extraction with our input values of the reflection coefficient and the length correction.

The "Pressure signal test" code generates a pressure field corresponding to the first higher mode $(1, 0)$ in a frequency range of $[10Hz\ ,\ 3000Hz]$. The cutoff frequency is $f_c^{1,0} = 1132Hz$ since the radius of the pipe is $a = 88mm$ (the same radius used by Q.Zhiping [1]). The signal is generated using the expression in equation 16:

$$p(a, \theta_{mic}, z_i, \omega) = P_{10}^{+}(\omega)[e^{-i\gamma_{10}z_i} + R_{10}^{A}e^{i\gamma_{10}z_i}]e^{i\theta_{mic}} \tag{40}$$

Where $P_{10}^{+}(\omega) = 1\ pa$ for all frequencies, $z_i = 0mm$ for the first measurements section and $z_i = s = 40mm$ for the second section, θ_{mic} is the azimuthal position of the microphone and γ_{10} is calculated using equation 14.
The magnitude of the artificial reflection coefficient is forced to a constant value $|R_{10}^{A}| = 3$ and the artificial length correction is a simple function of f and a:

$$\delta_{10}^{A} = \frac{a}{1 + f^2}10^6 \tag{41}$$

According to equation 27 the total artificial reflection coefficient at the open end of the pipe is:

$$R_{10}^{A} = -3e^{-2i\gamma_{10}\delta_{10}^{A}} \tag{42}$$

The program "*Read txt*" is not used in this test, because the pressure data generated by "*Pressure signal test*" are directly transferred to the program "*Modal extract*" since both of them are built with Matlab. The final result of this test is summarized in figure 12. According to the curves in figure 12 the post processing program "*Modal extract*" gives the exact results as expected in equations 42 and 41:

III.2.2.2 Matrix conditioning:

As mentioned in paragraph II.2.3.1, the condition in equation 29 should be fulfilled in order to have an invertible matrix. But even if the matrix is invertible, the solution could be very sensitive to errors. In order to check the sensitivity of the solutions to errors in the simulation, the matrix conditioning is calculated for the configuration where the distance $s = 40mm$ between the two measurement sections. Figures 13 and 14 shows that the matrix conditioning is very heigh at low frequency range because the wave-number is very small which means that the elements of the matrix are close to each other. The figures illustrate also the condition for invertibility mentioned in paragraph II.2.3.1 because we can notice that the conditioning is very high at particular frequencies called "forbidden frequencies". The forbidden frequencies depends on the distance s and the radius of the pipe a, in our case $s = 40mm$ and $a = 88mm$ and according to equation 29 the forbidden frequency for the plane mode is $4250Hz$ and $4398Hz$ for the mode (1.0) which correspond to the peaks of the conditionning. In figure 14 there is another peak located at $1132Hz$ which is the cut-off frequency of the mode (1.0), M.Abom gives in his paper [13] a frequency range around the cut-off frequency where the results are sensitive to errors by:
for mode (1.0):

$$1 < \frac{f}{f_{10}} < 1.033 \tag{43}$$

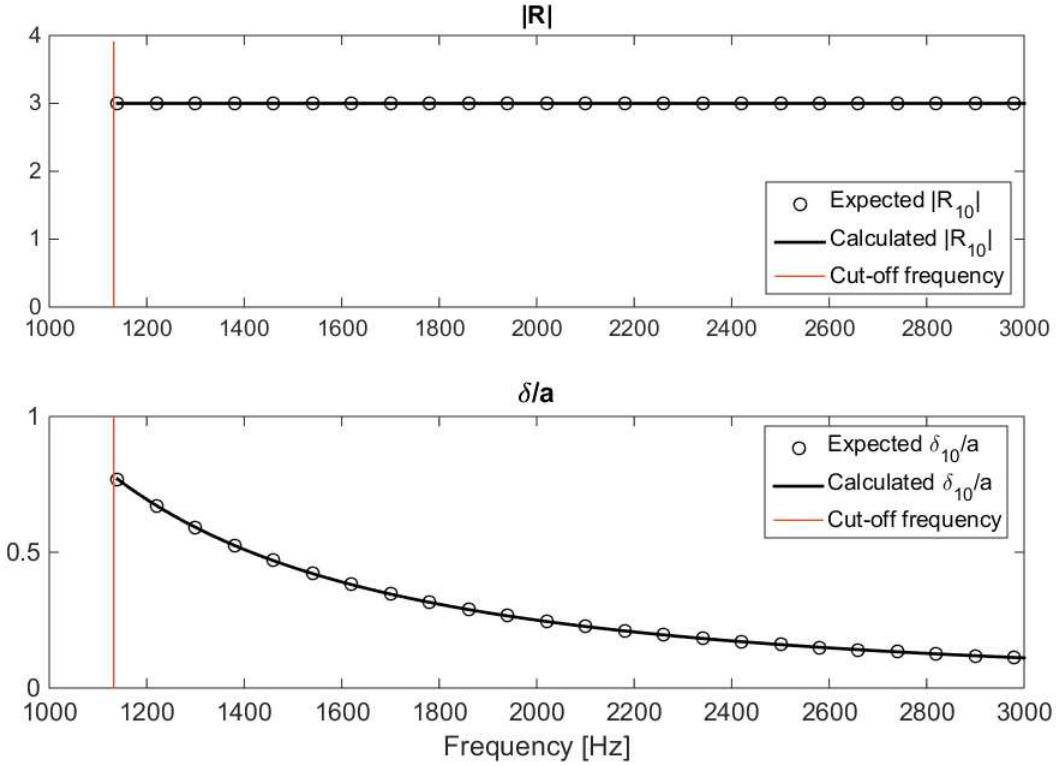

Figure 12 – Comparison between the expected results and the results calculated with the post-processing code

for mode mode (2.0):

$$1 < \frac{f}{f_{20}} < 1.012 \tag{44}$$

In order to verify that the measurement or simulation errors don't have an important impact on the results, we added noise to the calculated pressure at each microphone and we compared the results with and without noise. The noise used in this test is a random pressure δp limited to $\pm 3\%$ of the pressure measured at each microphone. Figure 15 shows that even with a bad matrix conditioning at low frequency range the noise doesn't introduce an important error.

In conclusion modal decomposition with two measurement sections method is sensitive to noise especially in low frequency range and near to modal cut-off frequencies, but it still a reliable method in our study since we are using numerical simulation and the signals are clean.

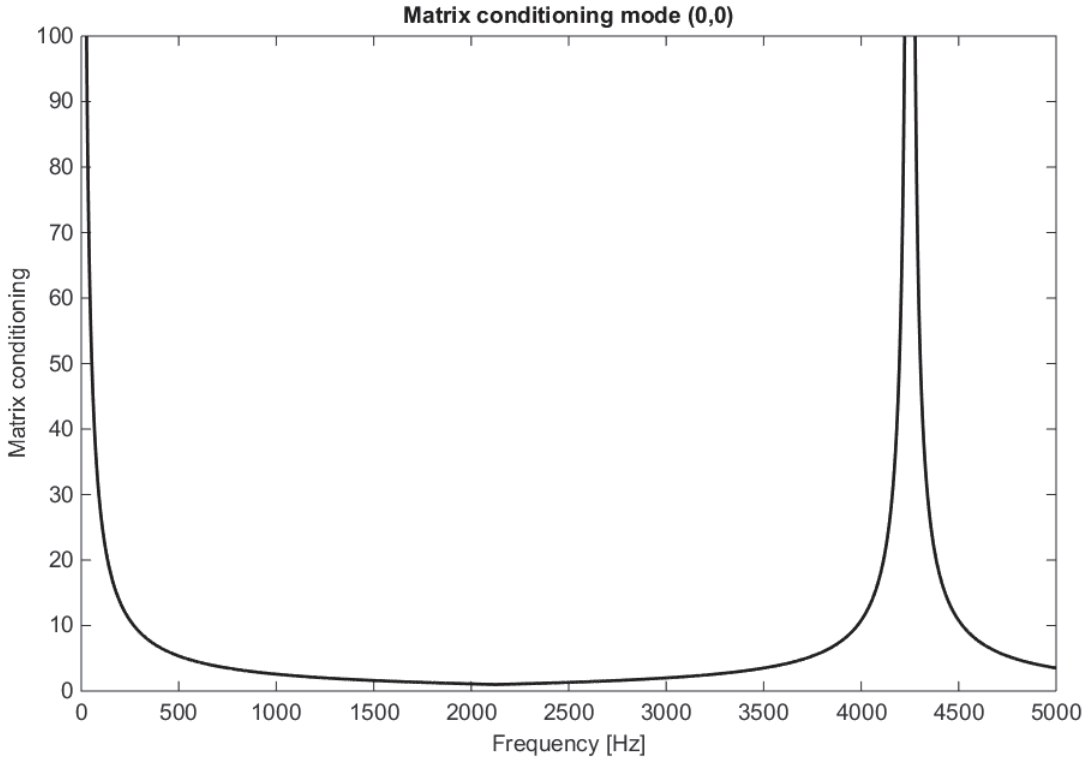

Figure 13 – Matrix conditioning for mode (0.0)

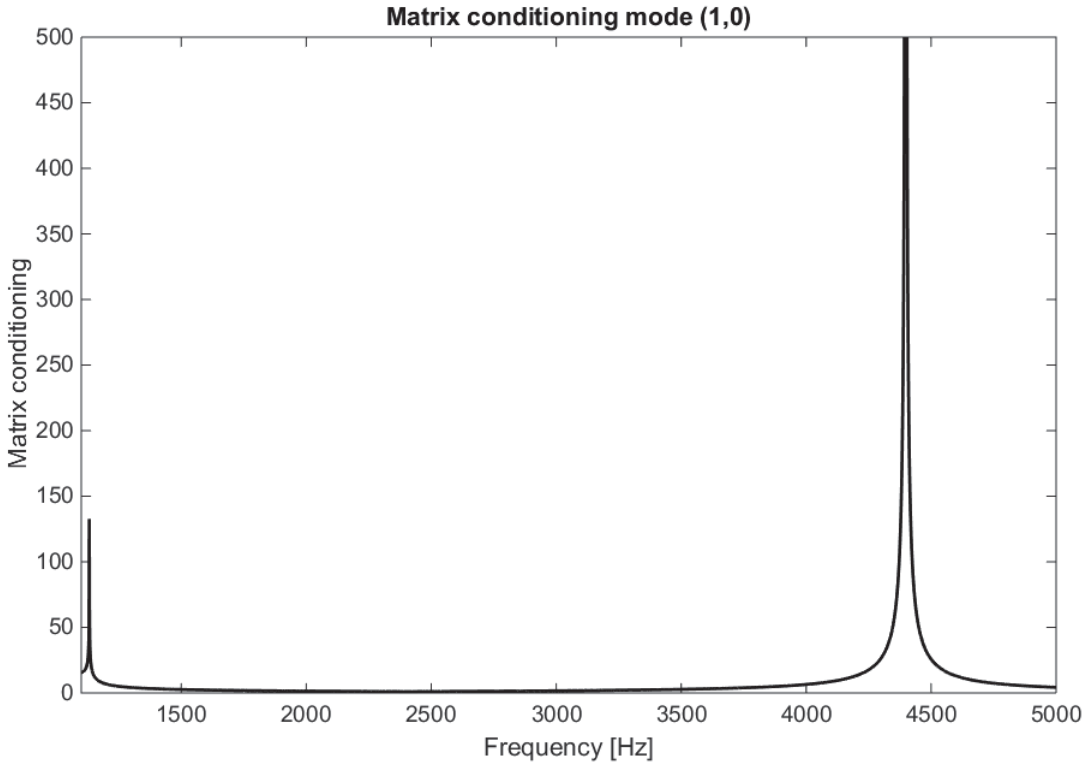

Figure 14 – Matrix conditioning for mode (1.0)

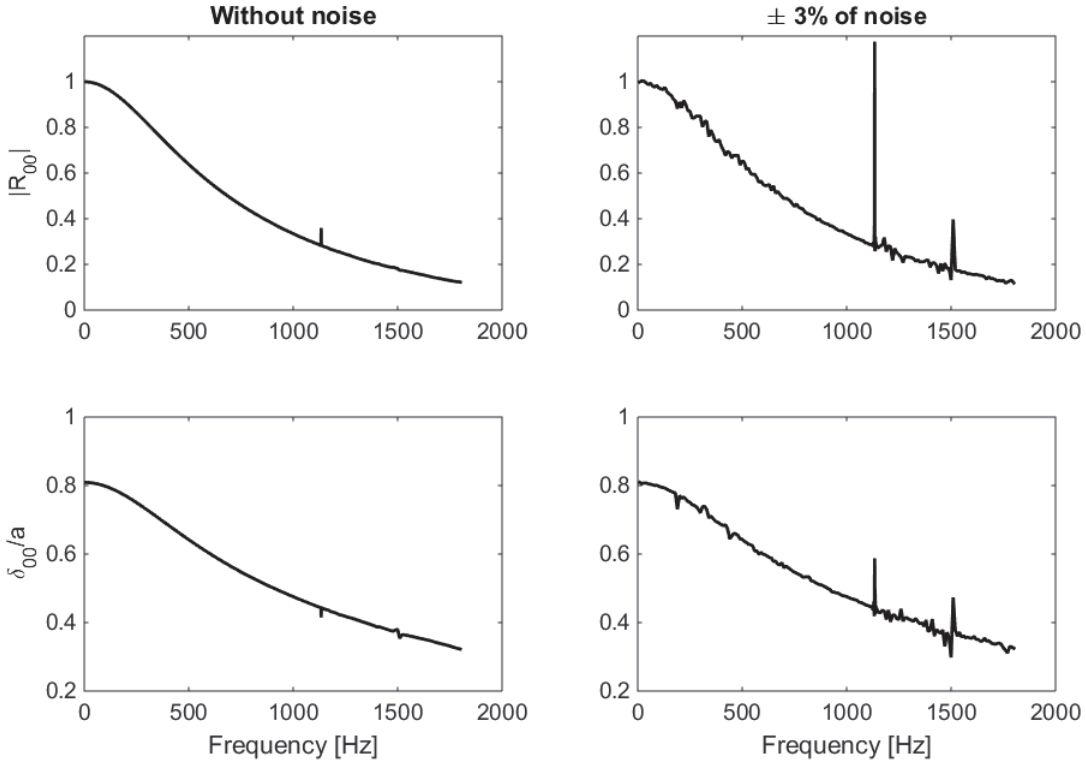

Figure 15 – The impact of noise on the reflection coefficient and length correction calculations

IV Sensitivity calculations:

In order to evaluate the sensitivity of our numerical model to the inputs, some sensitivity calculations have been performed on different parameters. These calculations will allow us to quantify the error induced by each input, then the choice of the parameters could be justified in the end.
The boundary conditions used in this paragraph are presented in section III.1.1

IV.1 Sensitivity calculations for the baffled pipe configuration:

All the sensitivity calculations in this paragraph are performed for the baffled guide configuration. In this case the geometry used in all the following calculations of this paragraph is based on two main parts: a half of a sphere with a radius R and a tube of radius a and length l as depicted in figure 16.

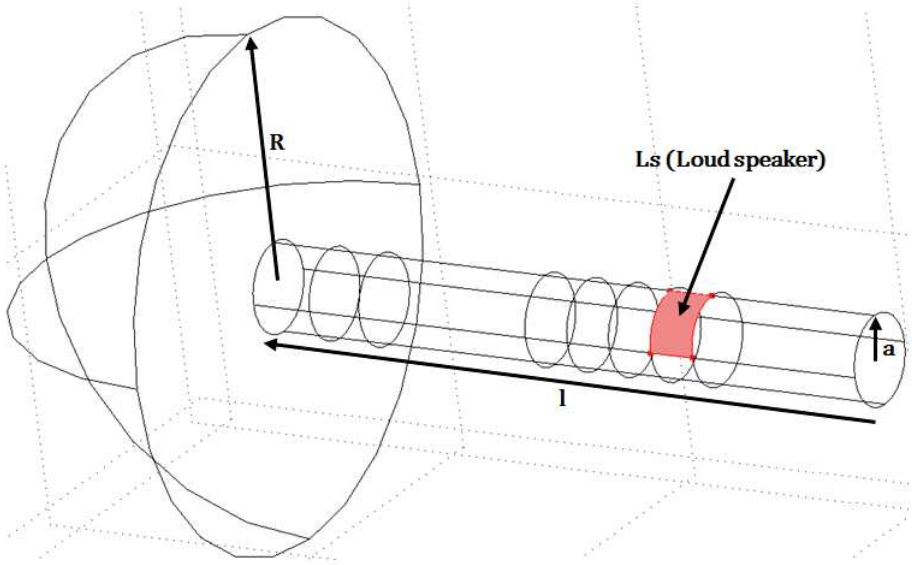

Figure 16 – Baseline geometry of the baffled guide

IV.1.1 Sensitivity to the sphere radius "R":

IV.1.1.1 Numerical model and parameters:

Even with a non-reflection condition on the external surface of the sphere, a small part of the pressure waves could be reflected toward the simulation domain. So the size of the sphere has an impact on the amount of the reflected pressure waves, especially in low frequency range, because in models with bigger spheres the waves are attenuated due to the geometrical spreading then the amplitude of the reflected waves will be much smaller. Moreover, the far field condition is well fulfilled in models with big spheres so the outgoing waves have almost the shape of the sphere when they reach the boundary of the finite/infinite domain. The main purpose of this sensitivity calculation is finding the minimum size of the sphere which has the minimum impact on the results. The parameters used in this sensitivity calculation are summarized in table 1.

Cases	R
Case 1	$R = 2m$
Case 2	$R = 1m$
Case 3	$R = 0.5m$
Case 4	$R = 0.2m$
Case 5	$R = 0.1m$

Table 1 – Parameters of sensitivity calculations, sensitivity to R: a= $0.088m$, $l = 1m$, mesh size=$0.04m$, frequency range$[10Hz, 300Hz]$, solver: $BiCGStab$

In this sensitivity analysis only low frequencies are simulated because the far field condition should be fulfilled for big wavelengths. At a low frequency range ($<< 1000Hz$) only the plane mode can propagate because the first cut-off frequency in our case is $1132Hz$, so by using the axi-symmetry properties of the problem, this sensitivity analysis is performed in 2D axi-symmetry geometry in order to reduce the calculation time especially for cases with $R > 1m$. Figure 17 shows the different boundary conditions used in this sensitivity calculation:

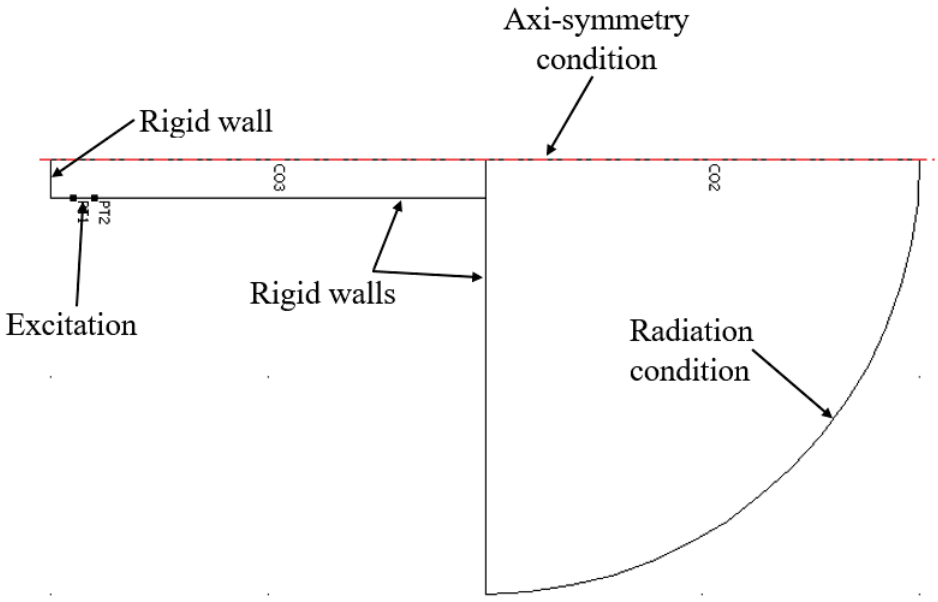

Figure 17 – Boundary conditions used in the calculations of the sensitivity to the size of the sphere

IV.1.1.2 Results and discussion:

The criterion of the comparison between the different calculation cases is the pressure at the pipe outlet of the first calculation case ($R = 2m$) assuming that the results stay almost the same for bigger radii ($R > 2m$). The relative error for a each case is calculated using the formula:

$$Error_i = \frac{\int_f |p(R_1) - p(R_i)|}{\int_f |p(R_1)|} \tag{45}$$

Where p is the pressure at the exit of the pipe and R_i is the sphere radius in the i^{th} case, for example: $p(R_1)$ is the pressure at the exit of the pipe with a sphere of a radius $R_1 = 2m$.The errors calculated for these four sensitivity cases are represented in the following bar chart in figure 18:

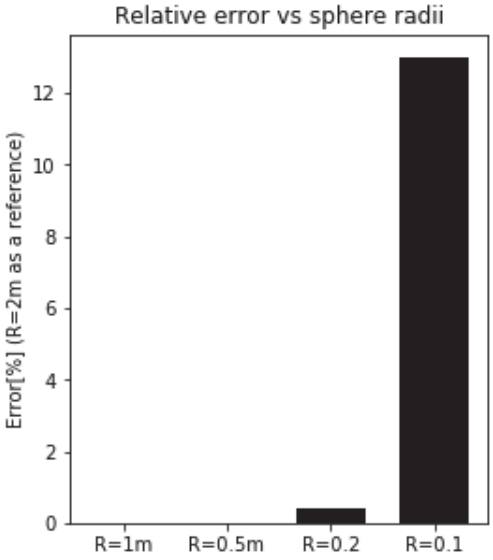

Figure 18 – Relative error calculated with different sphere sizes (see Eq. 45)

According to the bar chart the error is almost null for radii bigger than $0.2m$ and less than 1% for $R = 0.2m$ however the error exceeds 12% for $R = 0.1m$. In order to verify that the size of the sphere doesn't have an impact on the results for $(R > 0.2m)$, the pressure on the baffle is depicted on figure 19. According to figure 19, there is a good agreement between the pressure calculated with different models and the baseline model $(R = 2m)$ at $f = 50Hz$. Moreover the curves are completely superimposed at $f = 300Hz$ which means that the external surface of the sphere is "transparent" for the outgoing waves.

In conclusion, a model with a sphere radius bigger than $R = 0.2m$ is enough to model the semi-infinite space at the exit of the pipe.

IV.1.2 Sensitivity to the distance "LB" between the measurements section and the pipe open end:

IV.1.2.1 Numerical model and parameters:

There are two waves in the pipe: waves propagating toward the open end of the duct P^+, and the reflected waves propagating toward the bottom of the pipe P^-. As mentioned in section II.1, evanescent modes are attenuated exponentially in the pipe which means that evanescent modes could be present at the measurement section if the traveling distances are not sufficient and since the reflection coefficient is by definition $R_{mn} = \frac{P^-_{mn}}{P^+_{mn}}$ it could be affected in this case. The reflected waves travel the distance "L" between the loud speaker and the microphones and two times the distance "LB" between the open end of the pipe and the microphones section as depicted in figure 20, however the incoming waves travel only the distance L. The sensitivity analysis is performed on the distance "LB" and the distance "L" is set to $L = 1m$.

The parameters used in the different sensitivity cases for "LB" are summarized in table 2

Cases	LB
Case 1	$LB = 0.35$
Case 2	$LB = 0.6$
Case 3	$LB = 1.35$

Table 2 – Parameters of sensitivity calculations, sensitivity to LB: $R = 0.5m$, a= $0.088m$, $L = 1m$, mesh size=$0.04m$, frequency range$[700Hz, 1900Hz]$, solver: $BiCGStab$.

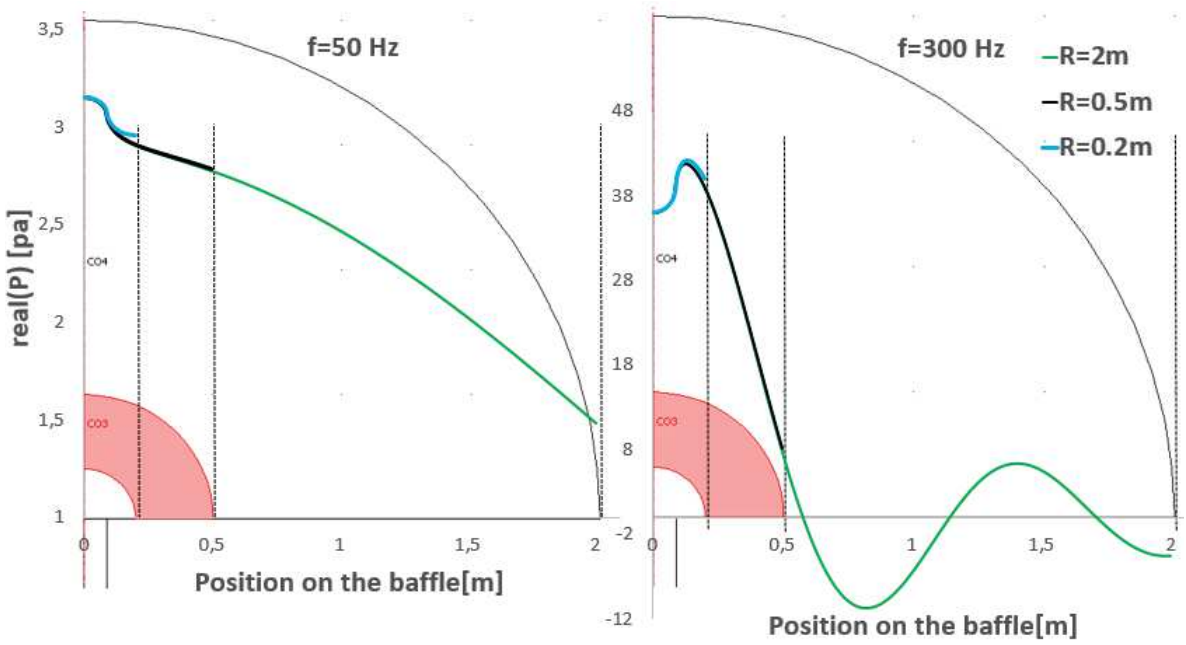

Figure 19 – The pressure along the baffle for models with $R = 2m$, $R = 0.5m$, $R = 0.2m$.

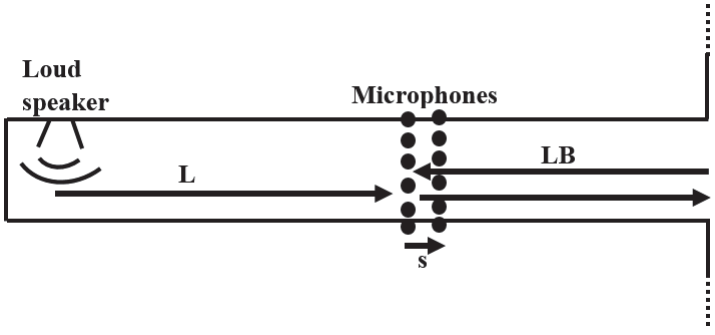

Figure 20 – The distances traveled by the waves inside the pipe

This sensitivity analysis is performed using the first higher mode (1,0). For the geometry used in this case the cut-off frequency of the mode (1,0) is $f = 1132Hz$, and since this mode has no axi-symmetry properties, the calculations are performed in 3D geometry using the same boundary conditions as the previous section [IV.1.1] except for the axi-symmetry condition.

IV.1.2.2 Results and discussion:

Figure 21 shows a comparison of the reflection coefficient modulus for the different cases. The reflection coefficient is calculated using "$Modal\_Extract$" code (see description in section III.2.1):

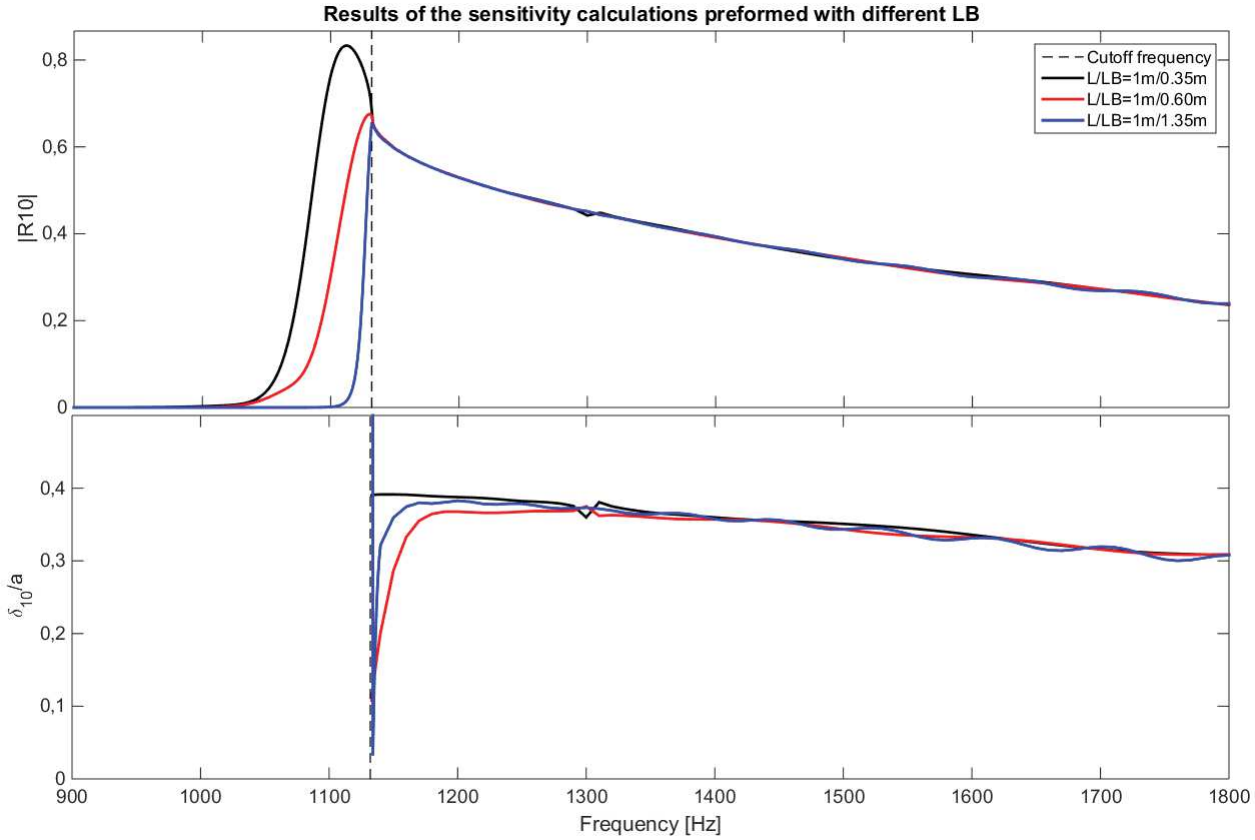

Figure 21 – Reflection coefficient of the mode (1,0) for different LB values $(0.35m, 0.6m, 1.35m)$

Figure 21 shows that for $LB = 0.35m$ and $LB = 0.6m$ the mode $(1, 0)$ is detected at frequencies lower than its theoretical cut-off frequency, which means that the reflected waves are not sufficiently attenuated when they reach the microphones at the measurement section. For $LB = 1.35$ the reflection coefficient modulus is non null only about $30Hz$ before the cut-off frequency and the slope change is much sharper. However after the cutoff frequency all the curves are superimposed.

In conclusion:

- Before the cutoff frequency: a distance $LB = 1.35m$ between the microphones and the open end is enough to keep only the propagating modes and reject the evanescent ones.
- After the cutoff frequency: The results are not sensitive to the distance LB because the mode signature is very strong (high modal pressure amplitude). The differences between the results of the length correction are located near to the cut-off frequency where the

sensitivity to errors is higher. Then since we are interested only in propagating modes (after the cutoff frequency) we can choose small distances for LB. In the experiments done by Zhiping QIU [1] the distance LB varies between $0.11m$ and $0.28m$ depending on the configurations (flanged, baffled or unbaffled pipe).

IV.1.3 Sensitivity to the boundary condition at the bottom of the pipe:

IV.1.3.1 Numerical model and parameters:

Theoretically the pipe is a semi-infinite duct, which means that the bottom of the pipe should be modeled with a non-reflection condition in order to keep only the reflections on the pipe walls and the open end of the pipe. But due to technical difficulties, the experiments done by Zhiping QIU [1] in his PhD are performed with a closed pipe (rigid bottom). The purpose of this paragraph is performing simulations with a closed pipe and non-reflection condition at the bottom of the pipe in order to show the impact of the bottom boundary condition on the results. The parameters used in this sensitivity analysis are summarized in the table 3

Cases	R	L	LB	a	BC at the bottom of the pipe	frequency range	Mesh size
Case 1	$0.3m$	$0.83m$	$0.12m$	$0.088m$	Rigid	$[10Hz, 1500Hz]$	$\frac{\lambda_{min}}{6}$
Case 2	$0.3m$	$0.83m$	$0.12m$	$0.088m$	Anechoic	$[10Hz, 1500Hz]$	$\frac{\lambda_{min}}{6}$

Table 3 – Parameters of sensitivity calculations, sensitivity to the boundary condition at the bottom of the pipe

IV.1.3.2 Results and discussion:

Figure 22 shows the presence of resonances in the closed pipe. The following expression gives approximated values of resonance frequencies:

$$f_r = \frac{(1+2N)c_0}{4L+0.8a} \tag{46}$$

Where $N \in \mathbb{N}$ and L is the pipe length.
for higher modes (mn) the resonance frequencies are given by the expression [1]:

$$f_r^{mn} = \frac{c_0}{2\pi}\sqrt{(\frac{(2N+1)\pi}{2L})^2 + (\frac{\alpha_{mn}}{a})^2} \tag{47}$$

Figure 23 shows that the boundary condition at the bottom of the pipe has almost no impact on the reflection coefficient even though resonances appear in the closed pipe, because the reflection coefficient is defined as a ratio of two waves amplitudes.
In conclusion, a rigid wall boundary condition changes the pressure field in the pipe but does not affect the reflection coefficient, and since the experiments of Zhiping QIU [1] are performed with finite pipe, a rigid bottom will be used in the following simulations.

IV.1.4 Sensitivity to the mesh grid:

IV.1.4.1 Numerical model and parameters:

The calculation time for a simulation is related to its number of degrees of freedom which is directly related to the mesh size and the geometry of the elements. The mesh grid has an impact not only on the calculation time but also on the accuracy of the results, the reason why its mandatory to perform a trad-off analysis to find a good compromise between the accuracy

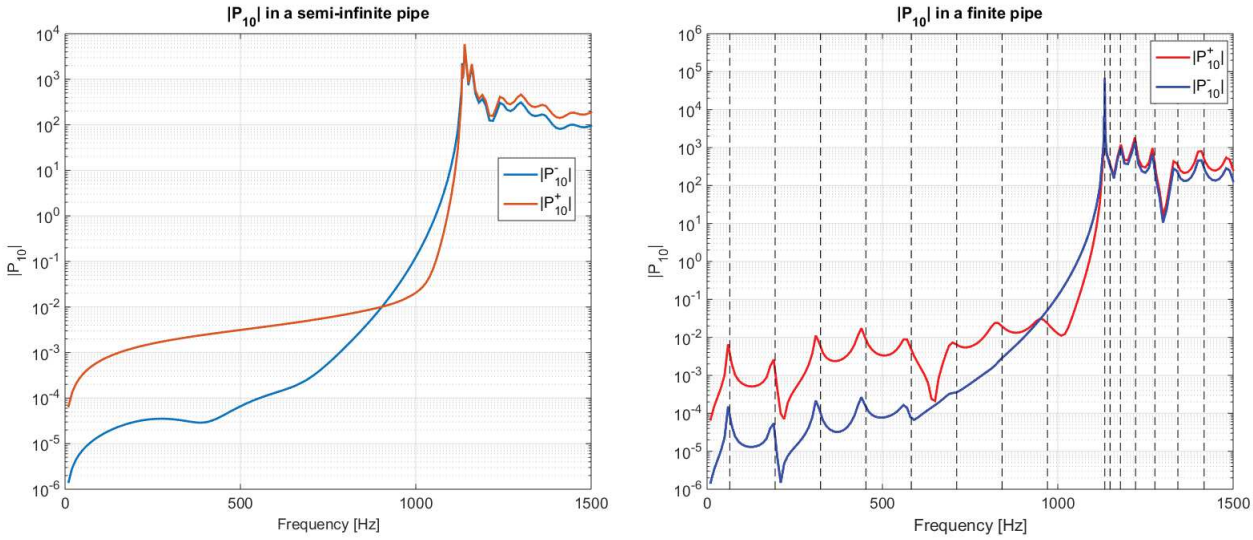

(a) Case 2, anechoic Bc "semi-infinite pipe" (b) Case 1, rigid Bc "finite pipe"

Figure 22 – Modal pressure $|P_{10}|$ in semi-infinite pipe and finite pipe

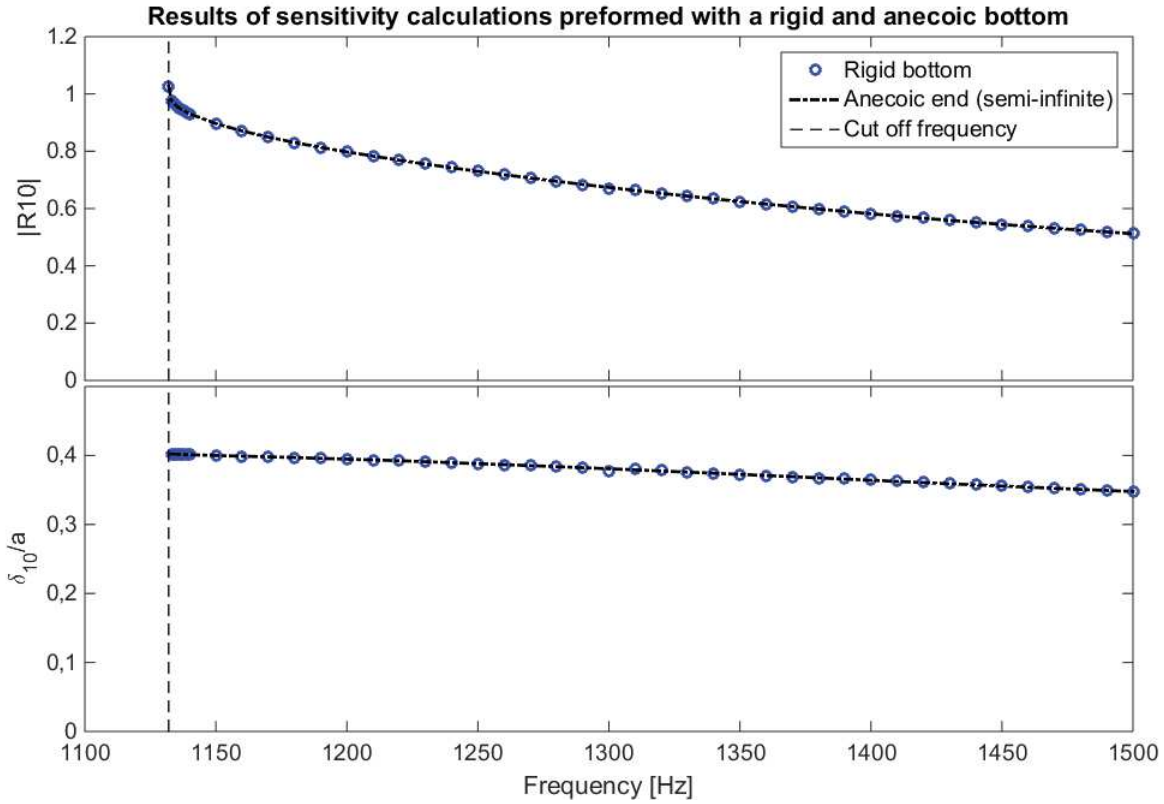

Figure 23 – Reflection coefficient of the mode (1,0) for a closed pipe and semi-infinite pipe

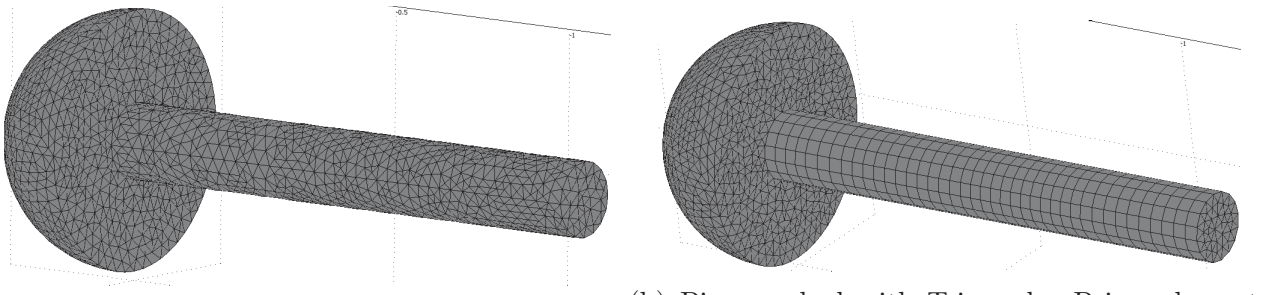

(a) The entire domain is meshed with Tetrahedral elements

(b) Pipe meshed with Triangular Prism elements and sphere meshed with Tetrahedral elements

Figure 24 – Geometries of the mesh grid used in the analysis of the sensitivity to the mesh grid

and the calculation time of our numerical model. Of course the maximum mesh size should be less than the minimum wavelength λ_{min}, in this sensitivity analysis mesh sizes of $h = \frac{\lambda_{min}}{3}$, $h = \frac{\lambda_{min}}{6}$ and $h = \frac{\lambda_{min}}{12}$ are used with two different elements' geometry "$Tetrahedral$" and a mix of "$Triangular\ Prism$" plus "$Tetrahedral$", figure 24 shows an example of these two mesh geometries.

The parameters used in this sensitivity analysis are summarized in table 4

Cases	Mesh size	Mesh grid	Number of elements
Case 1	$\frac{\lambda_{min}}{3}$	Mix	2 499
Case 2	$\frac{\lambda_{min}}{6}$	Mix	25 017
Case 3	$\frac{\lambda_{min}}{6}$	Tetrahedral	35 096
Case 4	$\frac{\lambda_{min}}{12}$	Mix	132 845
Case 5	$\frac{\lambda_{min}}{12}$	Tetrahedral	188 874

Table 4 – Parameters of sensitivity calculations, sensitivity to the mesh: $R = 0.3m$, a= $0.088m$, $L = 0.83m$, $LB = 0.12m$, frequency range $[1130Hz, 1500Hz]$, solver: $BiCGStab$.

IV.1.4.2 Results and discussion:

We can notice that by using a mixed mesh (Triangular Prism and Tetrahedral) the number of elements is reduced by about 28%. The figure 25 shows that the mesh grid has a minor impact on the reflection coefficient, however we can notice that a mesh size of $h = \frac{C}{6\,f_{max}}$ or less gives better results. In conclusion, all simulations in this study will be performed using a mixed mesh with maximum elements size of $h = \frac{C}{6\,f_{max}}$.

IV.2 Sensitivity calculations for the unbaffled pipe configuration:

All the sensitivity calculations in this paragraph are performed for the unbaffled guide configuration. In this case the geometry used in all the following calculations of this paragraph is based on two main parts: a complete sphere with a radius R centred on the outlet of the duct and a tube of radius a and length l as depicted in the figure 26.
The boundary conditions used in this paragraph are presented in section III.1.1.

IV.2.1 Sensitivity to the sphere radius "R":

IV.2.1.1 Numerical model and parameters:

The main purpose of this sensitivity calculation is finding the minimum size of the sphere which has the minimum impact on the results. The parameters used in this sensitivity calculation are

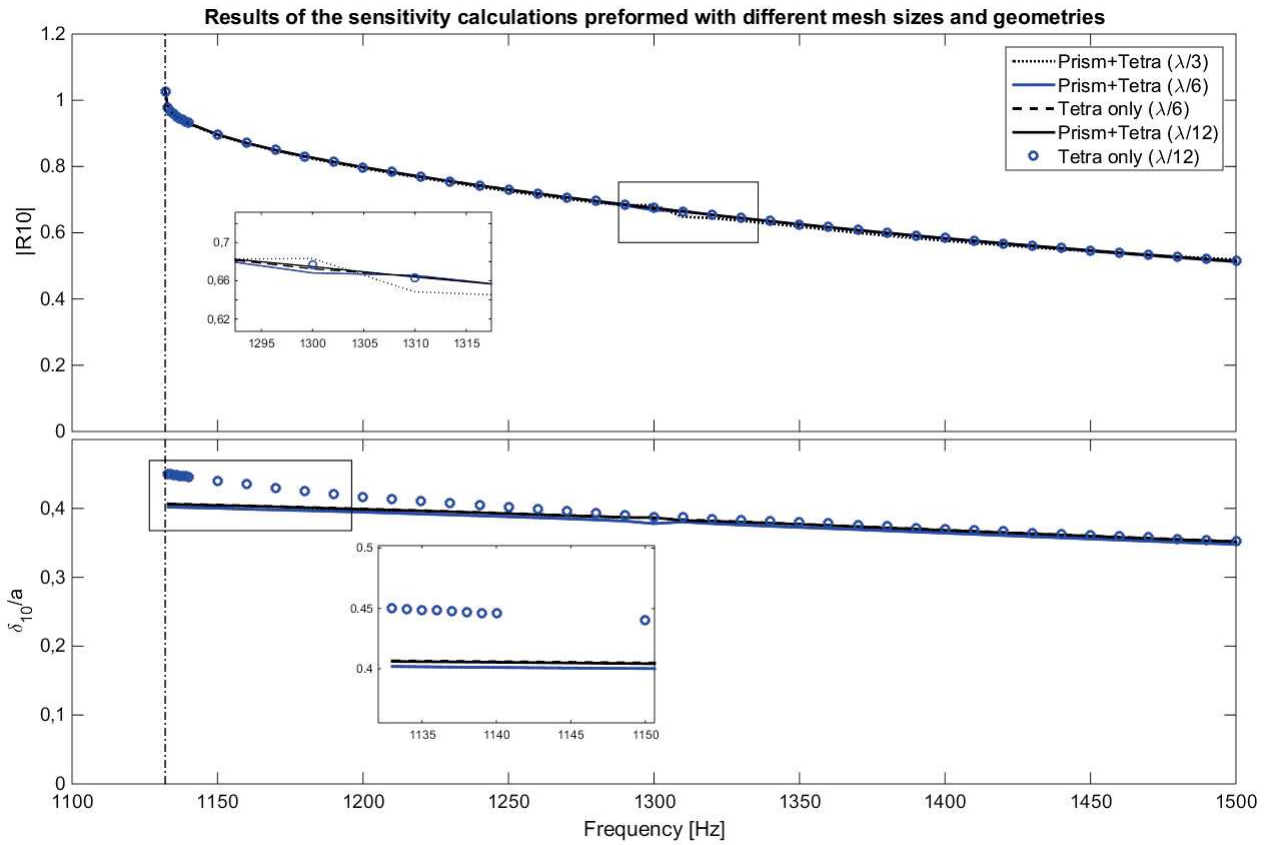

Figure 25 – Reflection coefficient of the mode (1,0) calculated with different mesh geometries and sizes

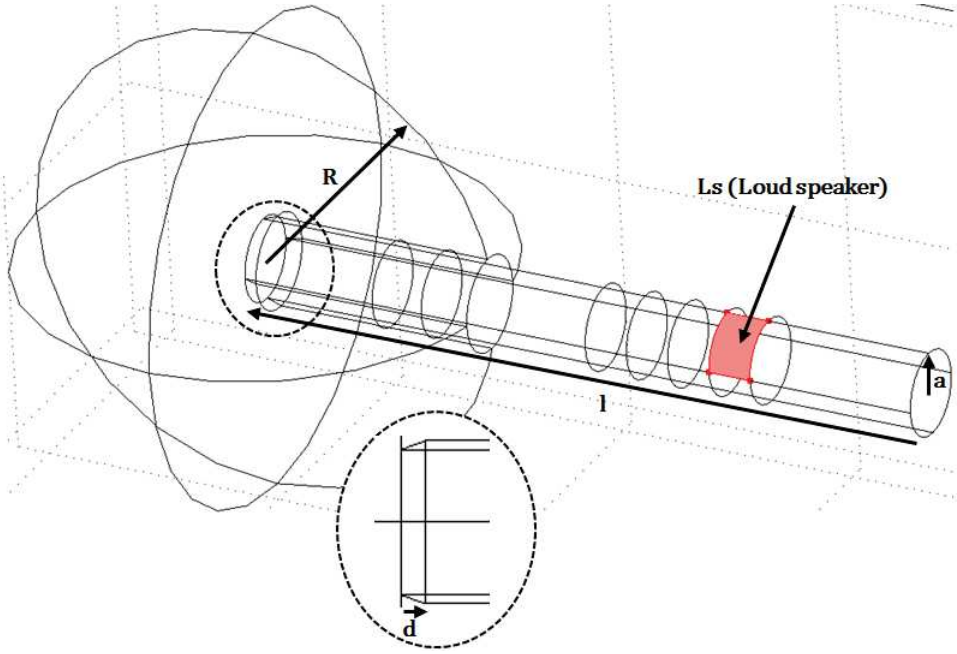

Figure 26 – Baseline geometry of the unbaffled guide

summarized in table 5.

Cases	R
Case 1	$R = 2m$
Case 2	$R = 1m$
Case 3	$R = 0.5m$
Case 4	$R = 0.3m$
Case 5	$R = 0.2m$

Table 5 – Parameters of sensitivity calculations, sensitivity to R: a= $0.088m$, $l = 1m$, frequency range $[10Hz, 300Hz]$, mesh size= $0.04m$, solver: $BiCGStab$.

These sensitivity calculations are performed in 2D axi-symmetry geometry for the same reasons explained in paragraph IV.1.1. Figure 27 shows the different boundary conditions used in this sensitivity calculation:

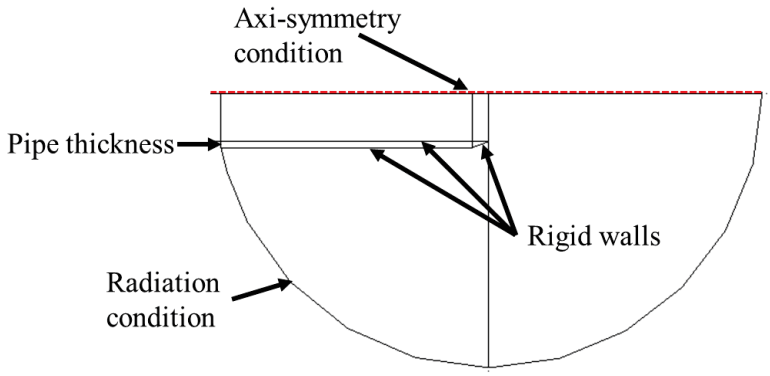

Figure 27 – Boundary conditions used in the calculations of the sensitivity to the size of the sphere

IV.2.1.2 Results and discussion:

The criterion of the comparison between the different calculation cases is the same criterion used in paragraph IV.1.1. The errors calculated for these four sensitivity cases are represented in the following bar chart in figure 28:

According to the bar chart the error is less than 4% for radii bigger than $0.3m$, however it exceeds 8% for $R = 0.2m$. In conclusion, a model with a sphere bigger than $R = 0.3m$ is enough to model the infinite space at the exit of the pipe if we accept 4% of error.

IV.2.2 Sensitivity to the geometry of the chamfer :

IV.2.2.1 Numerical model and parameters:

As depicted in figure 26, the unbaffled duct ends with a chamfer that simulate the unbaffled open end. A sensitivity calculations are performed on the geometrical parameters of the chamfer in order to show that the geometry of the chamfer doesn't have an important impact on the results. The chamfer is characterized by its angle α and width d. This sensitivity analysis is performed in two steps, firstly the width is set to $d = 30mm$ and the angle α is varied [10°,20°, 30°], secondly the angle α is set to 20° and the width is varied [$20mm$,$30mm$,$40mm$]. The parameters used in this sensitivity analysis are summarized in table 6:

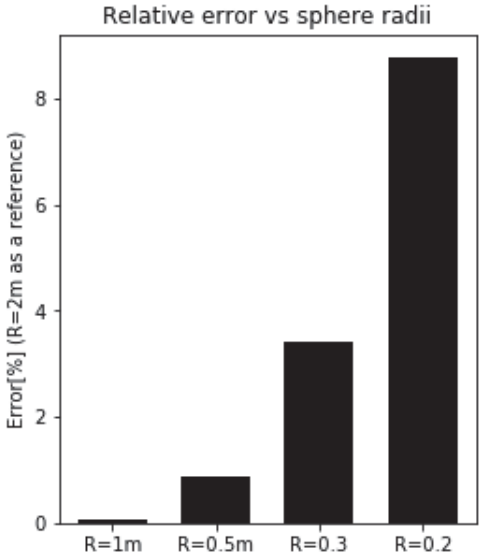

Figure 28 – Relative error calculated with different sphere sizes (see Eq. 45)

Cases	d	α
Case 1	$30mm$	$10°$
Case 2	$30mm$	$20°$
Case 3	$30mm$	$30°$
Case 4	$20mm$	$20°$
Case 5	$30mm$	$20°$
Case 6	$40mm$	$20°$

Table 6 – Parameters of sensitivity calculations, sensitivity to the chamfer geometry: $R = 0.3m$, a= $0.088m$, $L = 0.83m$, $LB = 0.28m$, frequency range $[1132Hz, 2000Hz]$, mesh size$\frac{\lambda_{min}}{6}$, solver: $BiCGStab$.

IV.2.2.2 Results and discussion:

According to figure 29 the angle of the chamfer has an impact on the results and it is more visible at high frequencies in the reflection coefficient modulus. However the impact on the length correction is more visible at low frequencies, because the conical surface of the chamfer acts like a small baffle at high frequencies especially when the angle is important and as a sharp edge at low frequencies. Figure 30 shows that the width d doesn't impact the results.

In conclusion, the geometry of the chamfer do have an impact on the reflection coefficient especially the angle α. In the following calculations and analysis, the geometrical parameters are set to the same geometry used by Zhiping [1] ($\alpha = 20°$, $d = 30mm$).

IV.2.3 Sensitivity to the mesh grid:

IV.2.3.1 Numerical model and parameters:

In this sensitivity analysis we consider only the region around the chamfer at the outlet of the pipe in order to represent the small details of the chamfer. Therefore the mesh refinement is located in a small sphere outside the pipe and a in small cylinder in the inside as depicted in figure 31. The mesh parameters in the rest of the geometry are the same as the previous section. Table 7 summarizes the parameters of this sensitivity calculation.

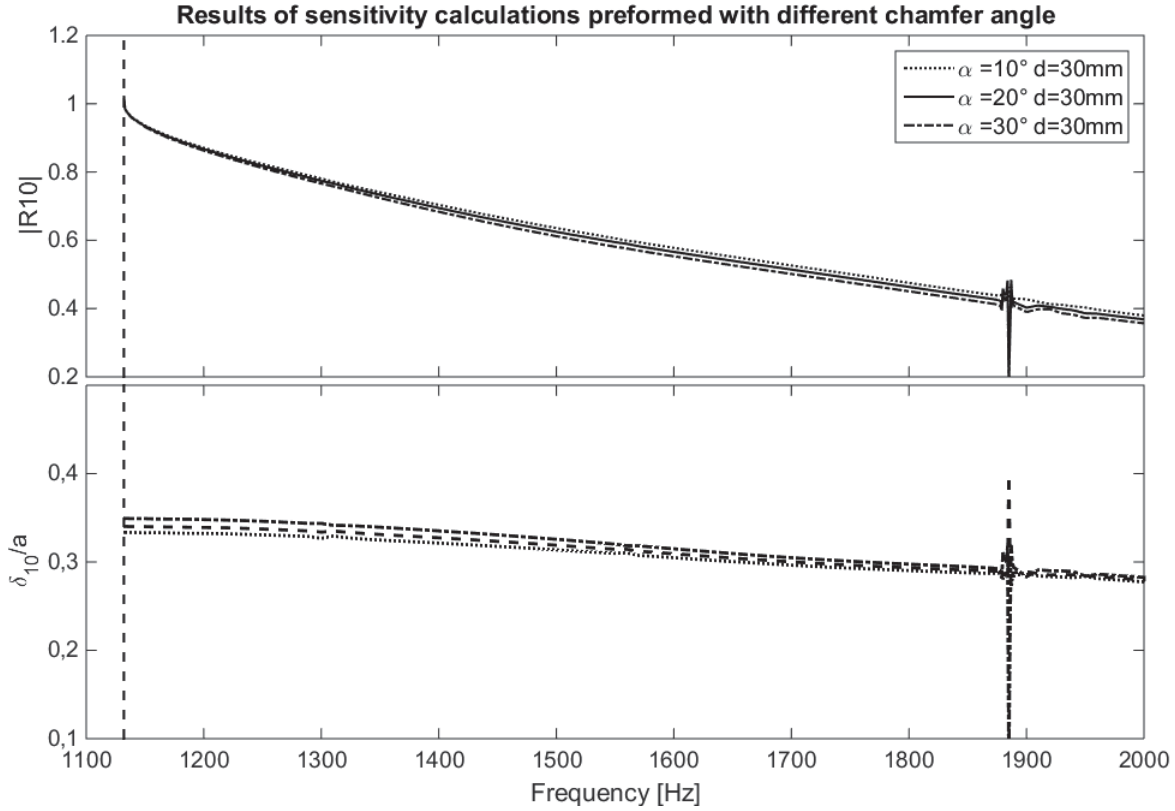

Figure 29 – Results of sensitivity calculations performed with different chamfer angle

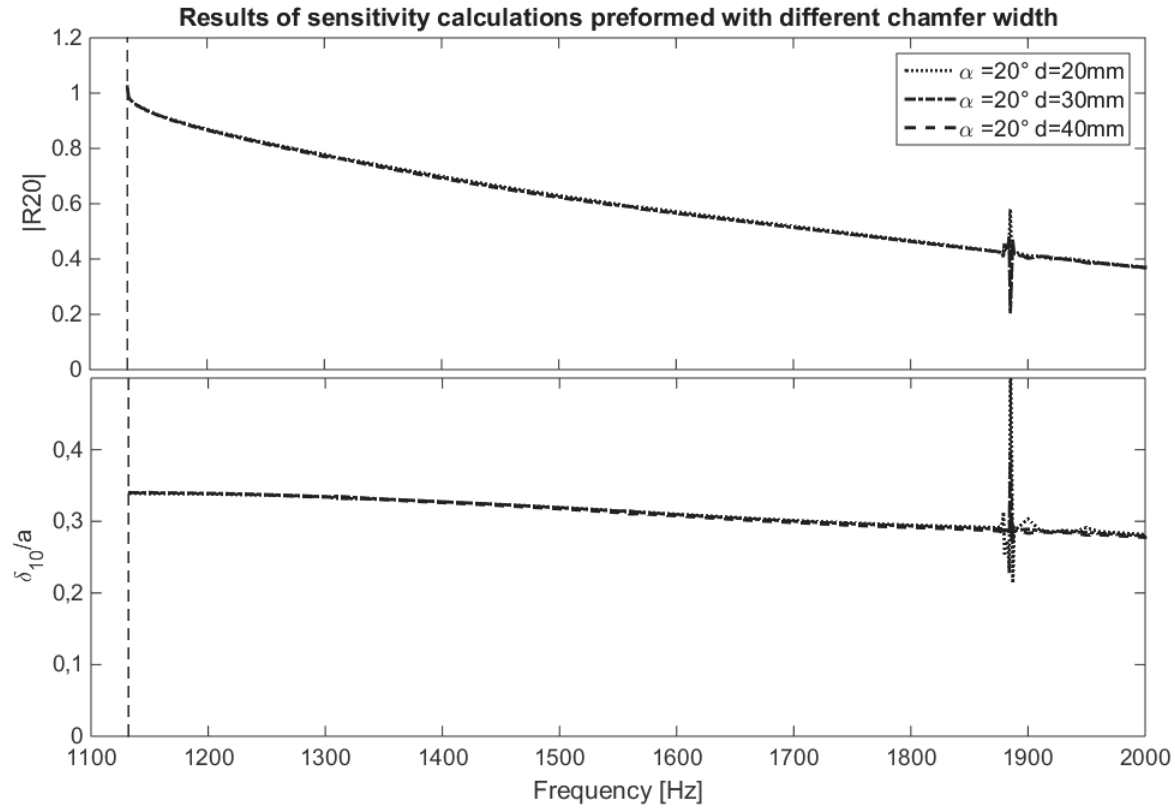

Figure 30 – Results of sensitivity calculations performed with different chamfer width

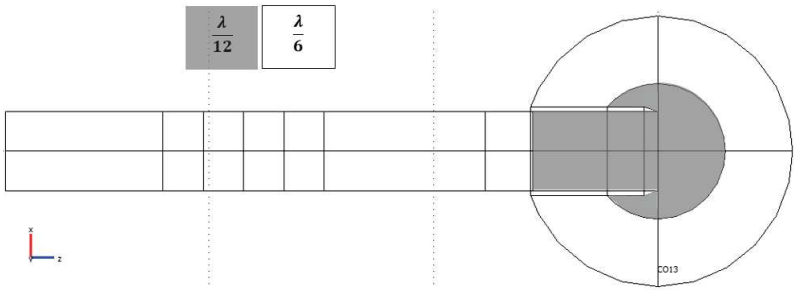

Figure 31 – Mesh refinement around the chamfer at the pipe outlet.

Cases	Mesh size	Mesh grid	Number of elements
Case 1	$\frac{\lambda_{min}}{6}$	Mix	70 293
Case 2	$\frac{\lambda_{min}}{8}$	Mix	102 197
Case 3	$\frac{\lambda_{min}}{12}$	Mix	161 428

Table 7 – Parameters of sensitivity calculations, sensitivity to the mesh grid: $R = 0.3m$, a= $0.088m$, $L = 0.83m$, $LB = 0.28m$, frequency range $[1132Hz, 2000Hz]$, solver: $BiCGStab$.

IV.2.3.2 Results and discussion:

Figure 32 shows that the mesh grid at the outlet of the pipe doesn't impact the reflection coefficient modulus, and it induces a maximum of 2.7% of error in length correction results which corresponds to $\approx 0.8mm$ of difference.

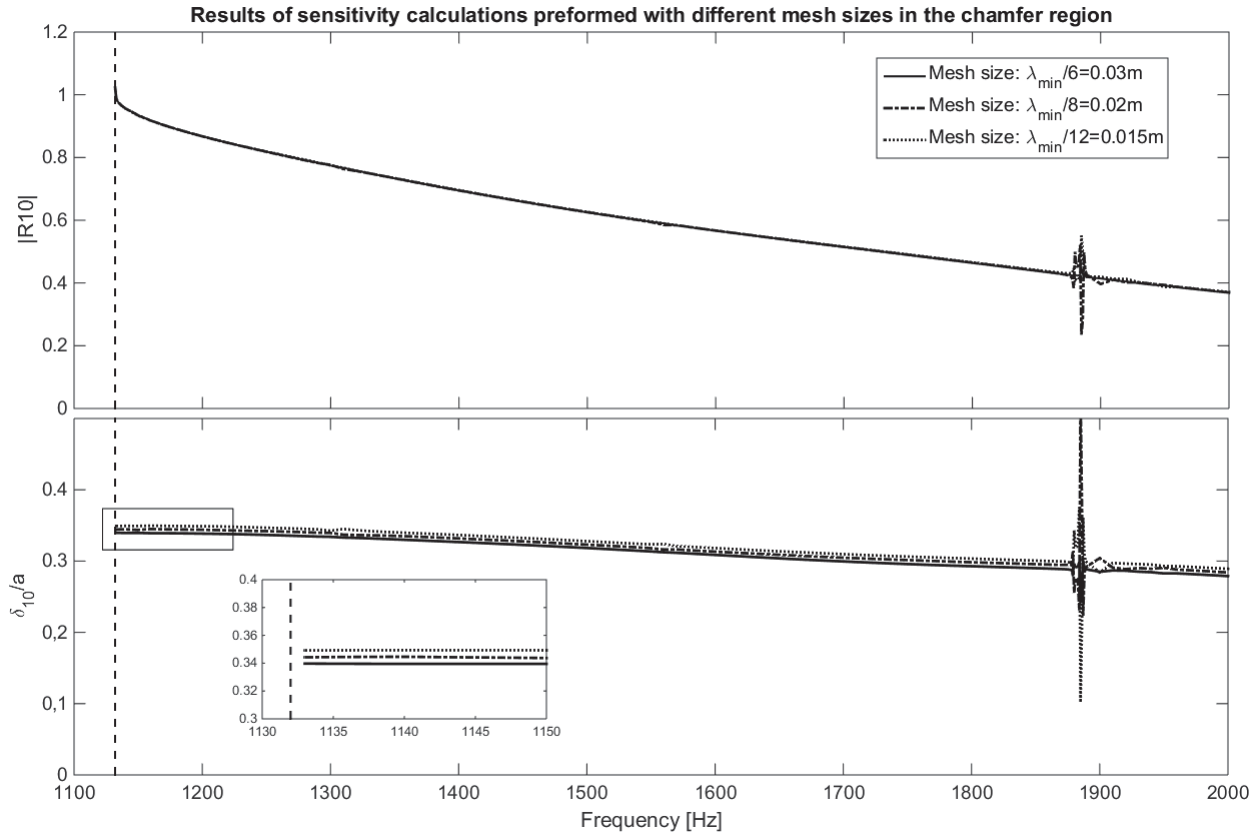

Figure 32 – Reflection coefficient of the mode (1,0) calculated with different mesh sizes at the outlet of the waveguide.

IV.3 Sensitivity calculations for the flanged pipe configuration:

The flanged pipe is a baffled duct with a finite screen (a flange). In this case, we used the same flange geometry in Zhiping's [1] experiments: a radius of $141mm$ and $15mm$ thick. The infinite space is modelled with a complete sphere with a radius R centred on the outlet of the duct as depicted in figure 33.

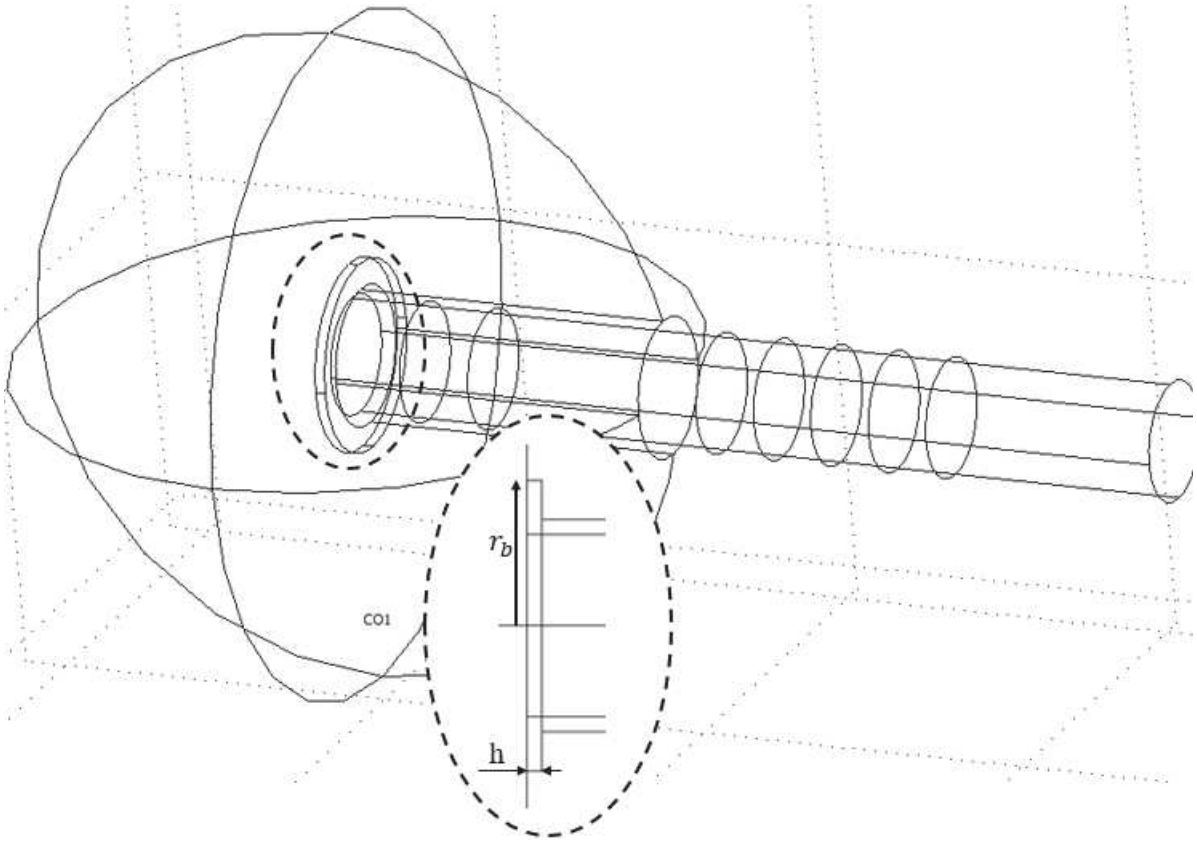

Figure 33 – Baseline geometry of the flanged guide, $h = 15mm$, $r_b = 141mm$.

IV.3.1 Sensitivity to the sphere radius "R":

IV.3.1.1 Numerical model and parameters:

Like the previous configurations, a sensitivity analysis is performed to show the impact of the sphere size on the results of the calculation. The parameters used in this sensitivity calculation are summarized in table 8.

Cases	R
Case 1	$R = 2m$
Case 2	$R = 1m$
Case 3	$R = 0.5m$
Case 4	$R = 0.3m$
Case 5	$R = 0.2m$

Table 8 – Parameters of sensitivity calculations, sensitivity to R: a= $0.088m$, $l = 1m$, mesh size=$0.04m$, frequency range$[10Hz, 300Hz]$, solver: $BiCGStab$

These sensitivity calculations are performed in 2D axi-symmetry geometry for the same reasons explained in paragraph IV.1.1. Figure 34 shows the different boundary conditions used in this sensitivity calculation:

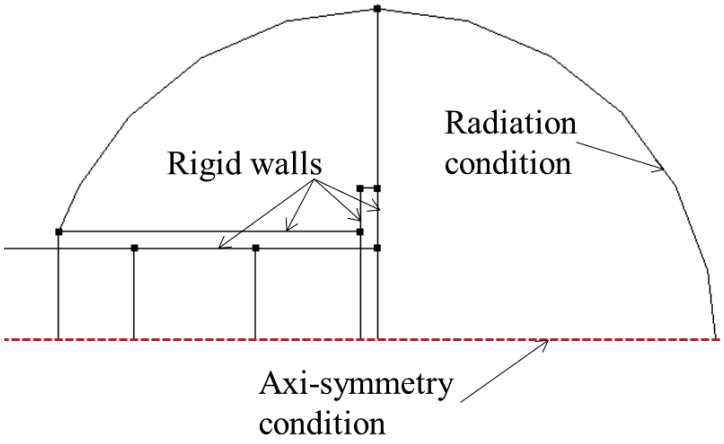

Figure 34 – Boundary conditions used in the calculations of the sensitivity to the size of the sphere

IV.3.1.2 Results and discussion:

The criterion of the comparison between the different calculation cases is the same criterion used in paragraph IV.1.1. The errors calculated for these four sensitivity cases are represented in the following bar chart in figure 35:

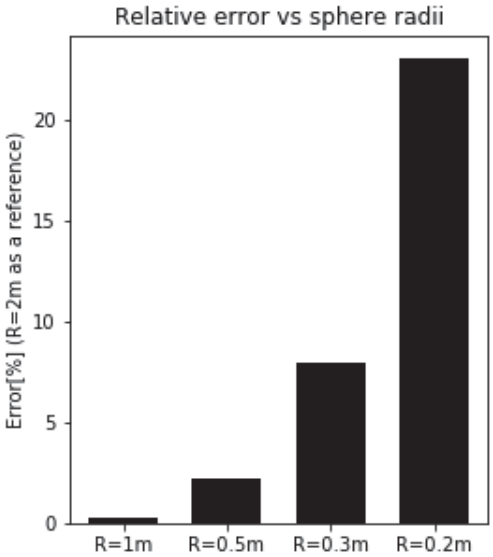

Figure 35 – Relative error calculated with different sphere sizes (see Eq. 45)

According to the bar chart the error is less than 3% for radii bigger than $0.5m$, however it exceeds 7% for radii smaller than $R = 0.3m$.
In conclusion, a model with a sphere bigger than $R = 0.5m$ is enough to model the infinite space at the exit of the pipe if we accept 3% of error. In our calculations we are limited by the computer specifications and we can ran simulations with a sphere radius up to $0.3m$ only, because if the number of degrees of freedom exceeds 8.10^5 dof the simulation crashes, the reason why we used a sphere with a radius of $0.3m$ for the flanged pipe.

IV.3.2 Sensitivity to the mesh grid:

IV.3.2.1 Numerical model and parameters:

Like the unbaffled configuration, in this sensitivity analysis we consider only the region around the flange at the outlet of the pipe. Therefore the mesh refinement is located in a small sphere outside the pipe and a small cylinder in the inside as depicted in figure 36. The mesh and geometry parameters are summarized in table 9.

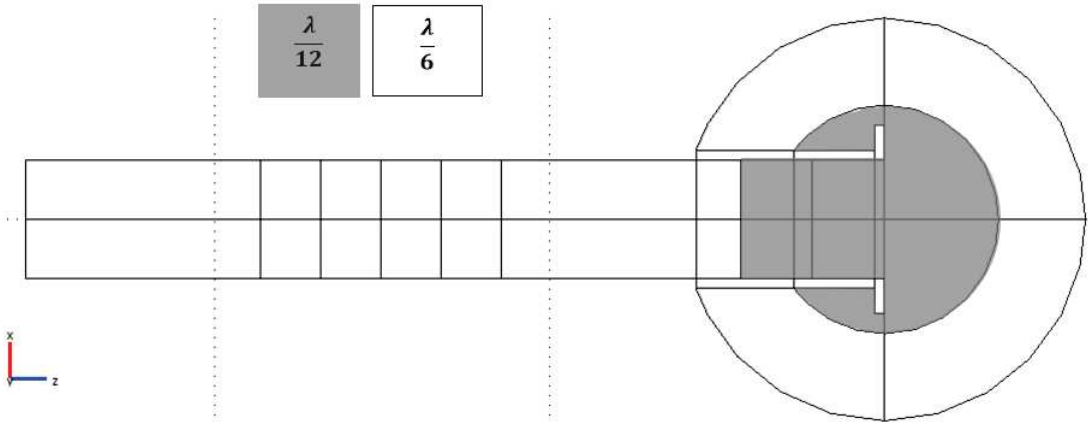

Figure 36 – Mesh refinement around the flange at the pipe outlet.

Cases	R	L	LB	a	frequency range	Mesh size	Mesh grid	Number of elements
Case 1	$0.3m$	$0.83m$	$0.11m$	$0.088m$	$[1130Hz, 2000Hz]$	$\frac{\lambda_{min}}{6}$	Mix	69 138
Case 2	$0.3m$	$0.83m$	$0.11m$	$0.088m$	$[1130Hz, 2000Hz]$	$\frac{\lambda_{min}}{12}$	Mix	165 832

Table 9 – Parameters of sensitivity calculations, sensitivity to the mesh grid

IV.3.2.2 Results and discussion:

Figure 37 shows that the mesh grid at the outlet of the pipe doesn't impact the reflection coefficient.

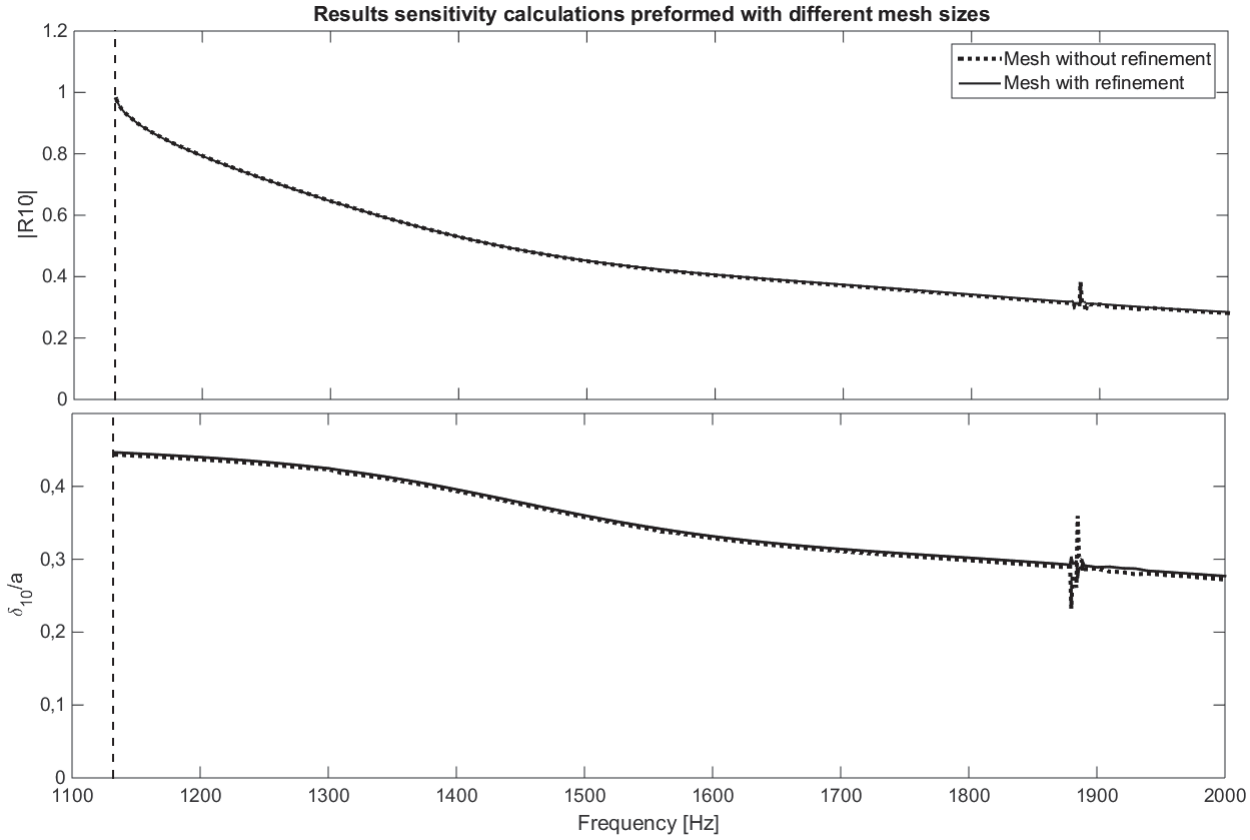

Figure 37 – Reflection coefficient of the mode (1,0) calculated with different mesh sizes at the outlet of the waveguide.

V Results of reflection coefficient and length correction calculations:

V.1 Numerical results of R_{m0} and δ_{m0}:

The simulations are performed with the same geometries used in the experimental work of Zhiping [1] in order to compare the numerical results to the experimental measurements. The considered configurations are also the same ones tested in the experimental work: the baffled pipe, the unbaffled pipe and the flanged pipe. Figure 38 shows the geometrical proprieties of the three configurations of the final simulation. The parameters of the final simulations are the same parameters used in sensitivity calculations:

- Software: Comsol Multiphysics;
- Computation algorithm: BiCGSTAB;
- Mesh size: 6 nodes per wavelength (minimum);
- Domain: $\rho_{air} = 1.23kg/m^3$ and $c_{air} = 340m/s$ without absorption and without mean flow;
- Boundary conditions: as described in section III.

Figure 39 shows the total pressure field calculated by Comsol Multiphysics without modal decomposition. The calculated pressure is a combination of different modes, all mixed in one complex pressure field (see figure 39 a), even though it's possible to find particular frequencies where a single mode is dominant (see figure 39 b, c and d). To propagate only one mode, the excitation should be controlled in order to generate the signature of that mode only. This method is not used in the main simulations but it's studied in appendix (B).

Since the objective of this study is the calculation of the multimodal reflection coefficient a modal decomposition is performed using Matlab codes described in section III.2.1. After the modal decomposition, the results obtained for the three configurations are depicted in figures 40 and 41. Figure 40 shows the reflection coefficient modulus of the plane (1.0) mode and the two first higher modes (1.0) and (2.0), and figure 41 shows the correponding length correction (the phase).
We can notice that the calculated reflection coefficient modulus and the length correction of the plane mode are in a good agreement with the results given by Norris and Sheng [6]. Another remark could be made on the reflection coefficient modulus of the plane mode for the flanged pipe, in figure 40 we can notice that the blue curve is closer to the reflection coefficient modulus of the unbaffled pipe at low frequencies since the wavelength is much bigger than the flange dimensions and at higher frequencies the curve tends to join the curve of the baffled pipe because the wavelength gets smaller and the flange could be compared to an infinite baffle. For the length correction, figure 41 shows that the impact of the outlet geometry on length correction is more visible for the plane mode than the higher modes. We can notice also that the curves of the length correction of higher modes tend tend to join the plane mode curve at high frequency range.
The dashed vertical lines mark the region where the results are more sensitive to errors as seen in paragraph III.2.2.2. However we can notice some fluctuations even in regions where the results are supposed to be insensitive to noise like the peak at $f = 1500Hz$. By examining the modal pressure amplitude of the outgoing wave and the reflected one in figure 42, we can see that these fluctuations are located at frequencies where the modal pressure amplitudes are at

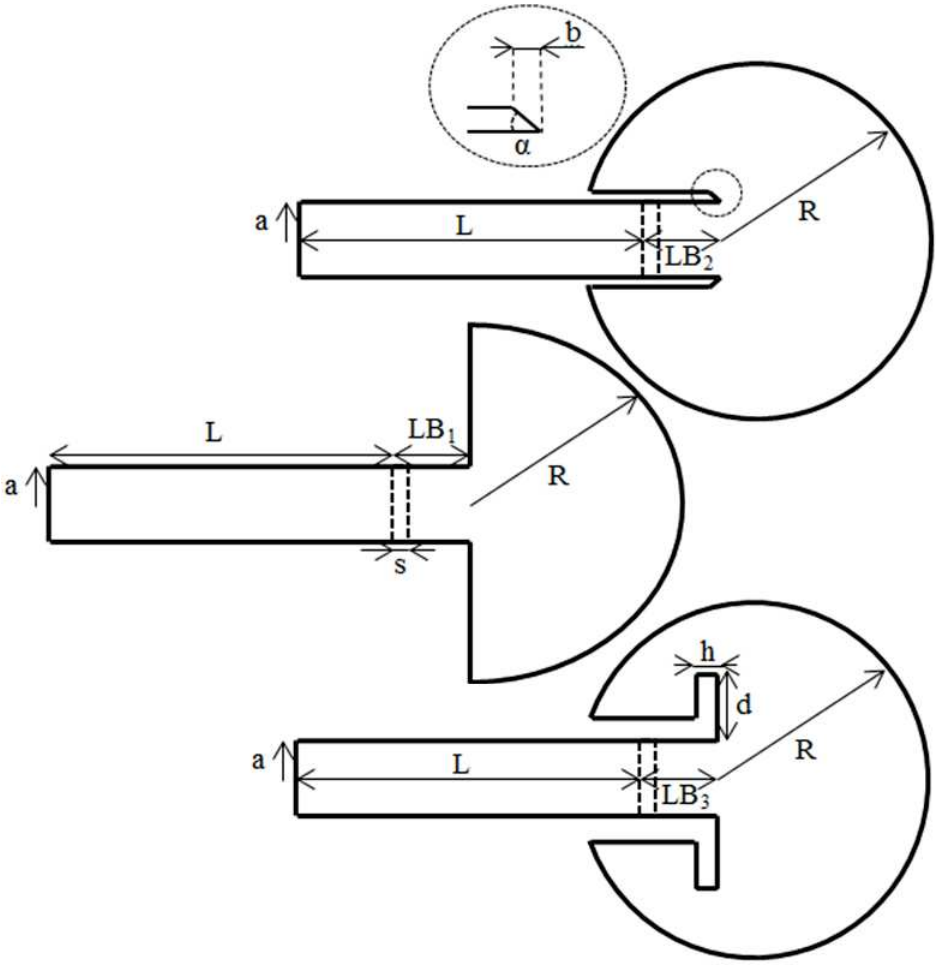

Figure 38 – Geometries used for the final simulations: a= $0.088m$, $L = 1.21m$, $LB_1 = 0.12m$, $LB_2 = 0.28m$, $LB_3 = 0.11m$, $R = 0.3m$, $b = 30mm$, $d = 53mm$, $h = 15mm$, $s = 40mm$, $\alpha = 20°$.

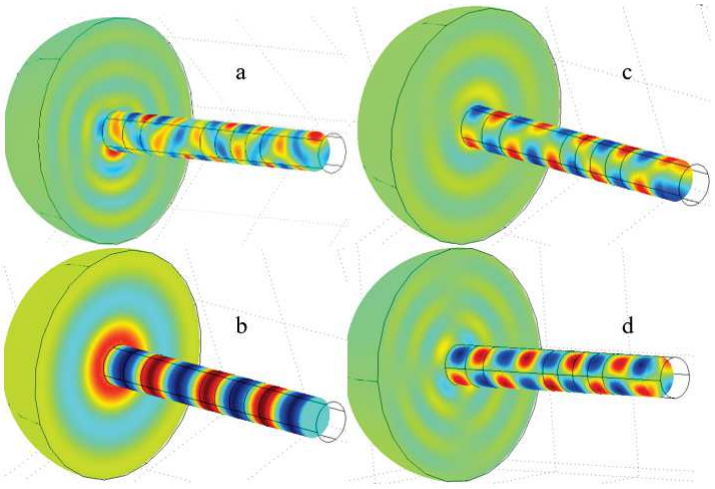

Figure 39 – Total pressure field in the baffled pipe without modal decomposition, a: combination of many modes at 2350Hz, b: plane mode is dominant at 1000Hz, c: mode (1.0) is dominant at 1760Hz and d: mode (2.0) is dominant at 2250Hz.

a minimum, which means that the signature of the mode is too weak compared to numerical errors, the reason why the results are perturbed at these particular frequencies. The modal pressure amplitude is at a minimum when the loudspeaker doesn't excite the mode efficiently which is the case when the excitation is located at a pressure node. Since our pipe is closed at the bottom, the pressure nodes are located at odd multiples of one fourth of a wavelength $\frac{(2n+1)\lambda}{4}$ as depicted in figure 43, because there is always a maximum pressure at the rigid bottom.

Let's take for example the minimum pressure of the plane mode. In our case, the loudspeaker is located at $LA = 0.395m$ from the rigid bottom of the pipe, in this case the loudspeaker is at a pressure node when $f = f_{min} = \frac{(2n+1)c_0}{4LA}$, these frequencies are marked by vertical dashed lines in figure 42.

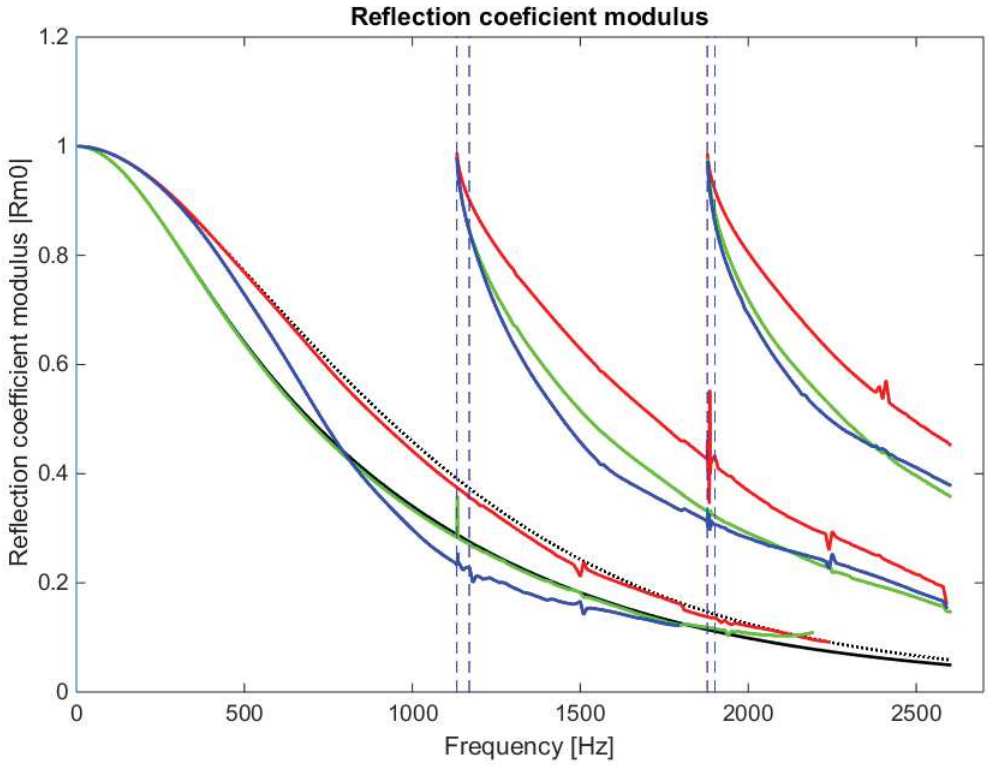

Figure 40 – Calculated reflection coefficient modulus: the black solid curve corresponds to the baffled pipe by Norris and Cheng, the black dashed curve corresponds to the unbaffled pipe by Norris and Cheng, red curves correspond to the unbaffled pipe, green curves correspond to the baffled pipe, the blue ones correspond to the flanged pipe and the dashed vertical lines marks the regions where the results are more sensitive to errors.

Remark 1:

Since the plane mode and the first radial mode (0.1) have the same radial signature on the circumference of the pipe ($r = a$) the modal decomposition using only two measurement sections can't distinguish between the mode (0.0) and (0.1), the reason why the calculation of the plane mode is limited to frequencies before the cut-off frequency of the mode (0.1).

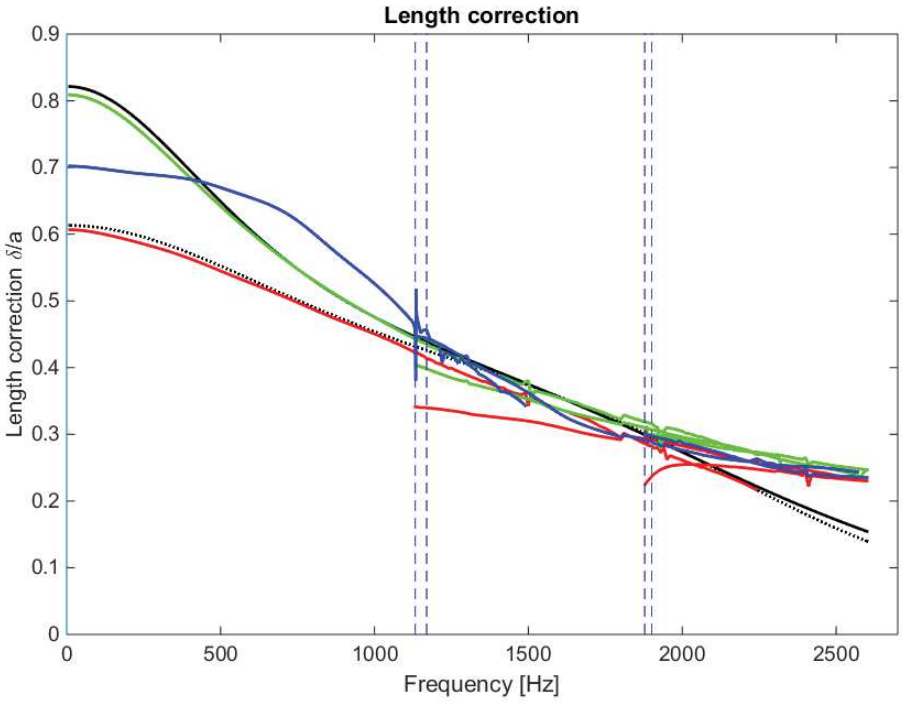

Figure 41 – Calculated length correction: the black solid curve corresponds to the baffled pipe by Norris and Cheng, the black dashed curve corresponds to the unbaffled pipe by Norris and Cheng, red curves correspond to the unbaffled pipe, green curves correspond to the baffled pipe, the blue ones correspond to the flanged pipe and the dashed vertical lines marks the regions where the results are more sensitive to errors.

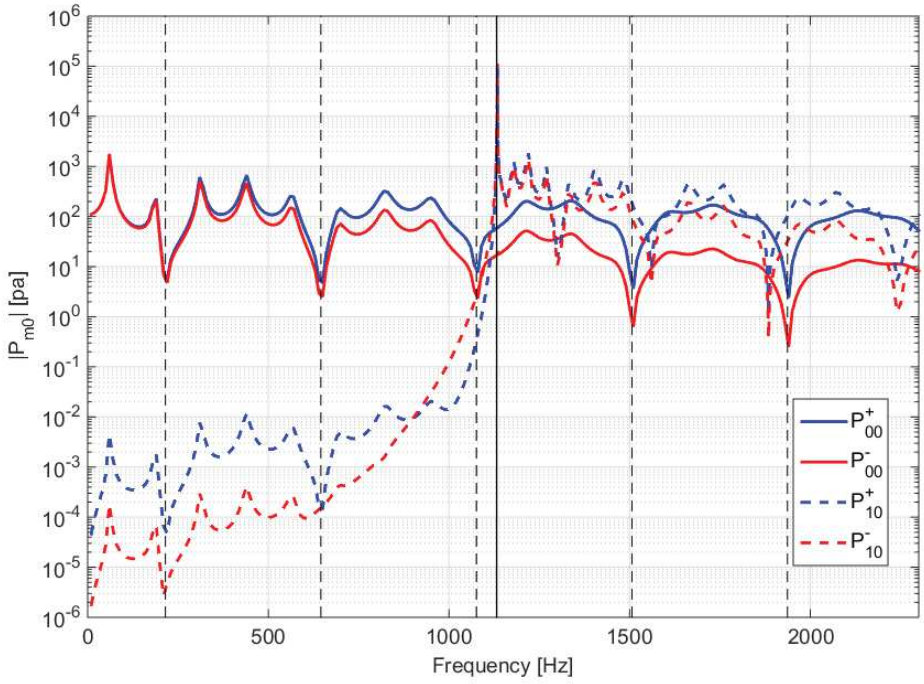

Figure 42 – Modal pressure amplitude for the baffled pipe configuration, P^+: outgoing wave, P^-: reflected wave.

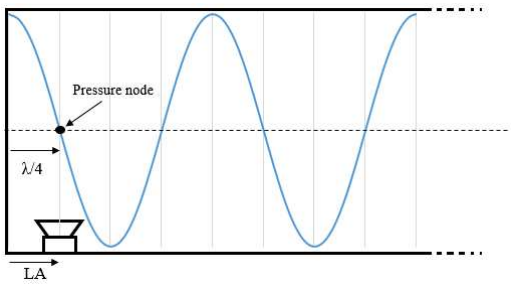

Figure 43 – Location of pressure nodes in a closed waveguide.

Remark 2:

By examining the modal pressure amplitude of the plane mode, we noticed that the length correction could be visualized an measured graphically on the pressure plot because we noticed that the reflection occurs at a minimum pressure region which means when the real part of the pressure field is at a minimum (the first minimum outside the pipe). Therefore, by measuring graphically, in figure 44, the distance between the pipe outlet (black solid vertical line) and the following first minimum of pressure (black dashed vertical line) we find the corresponding length correction. In figure 44 this graphical method is tested for two different frequencies $500Hz$ and $1000Hz$, the difference between the graphical measurement and the calculated value of δ_{00} is only 4.3% ($1.8mm$) at $500Hz$ however the graphical measurement gives the same value as the calculations at $1000Hz$.

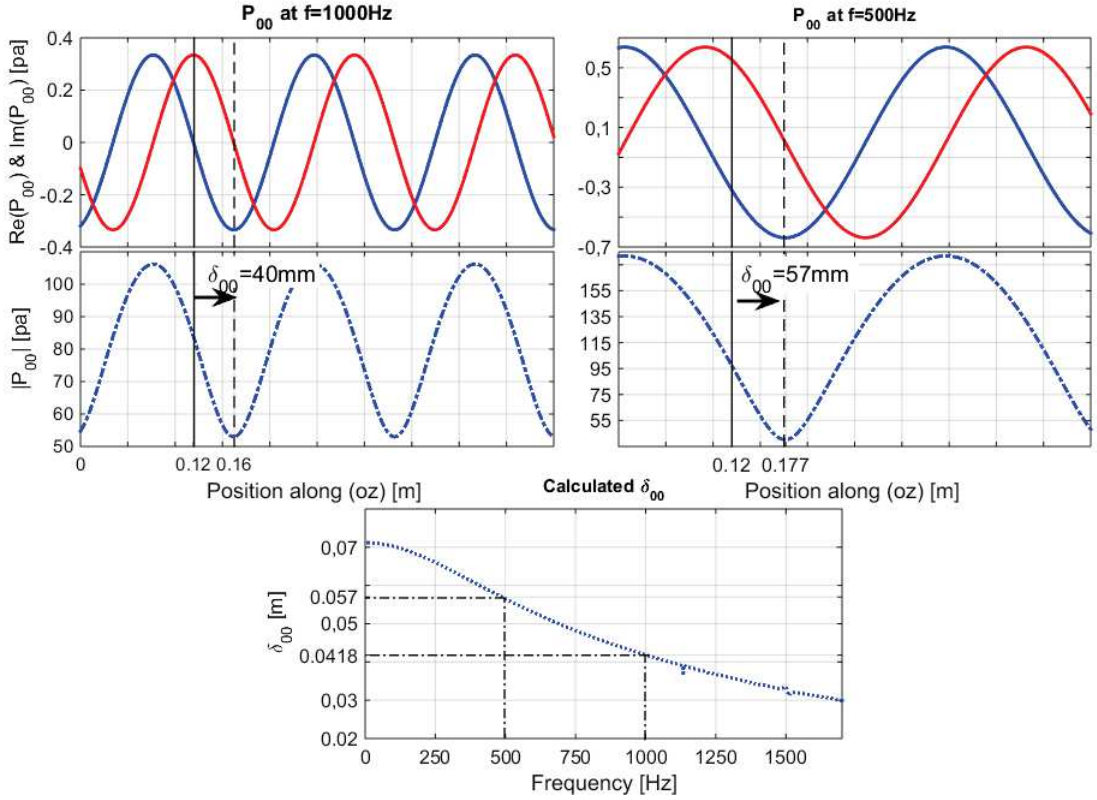

Figure 44 – Measuring δ_{00} graphically: the vertical black solid and dashed lines mark respectively the position of the pipe outlet and the reflection position, solid red and blue curves correspond respectively to $\Im(P_{00})$ and $\Re(P_{00})$, the blue dashed curves correspond to $|P_{00}|$ and blue dotted curve corresponds to the calculated δ_{00}.

V.2 Comparison of numerical results and experimental measurements:

As stated in the introduction, the main goal of the numerical simulations in this study is to support the results of the experimental work done by Zhiping [1] in his PhD at "Institut Pprime" laboratory.
The results of the numerical simulations and the experimental measurements of the reflection coefficient modulus are depicted in Figure 45. Numerical simulations and experimental measurement are in good agreement. We can make the same remark for the reflection coefficient of the flanged pipe as seen in the previous paragraph, where the reflection coefficient of the plane mode for the flanged pipe is closer to the reflection coefficient of the unbaffled pipe at low frequencies and tends to join the reflection coefficient of the baffled pipe when the frequencies get higher. We can also notice that the intersections between the reflection coefficient of the flanged and the baffled pipe (the blue and the green curves) of the numerical simulation are close to the intersections in the experimental curves (maximum 30Hz apart).

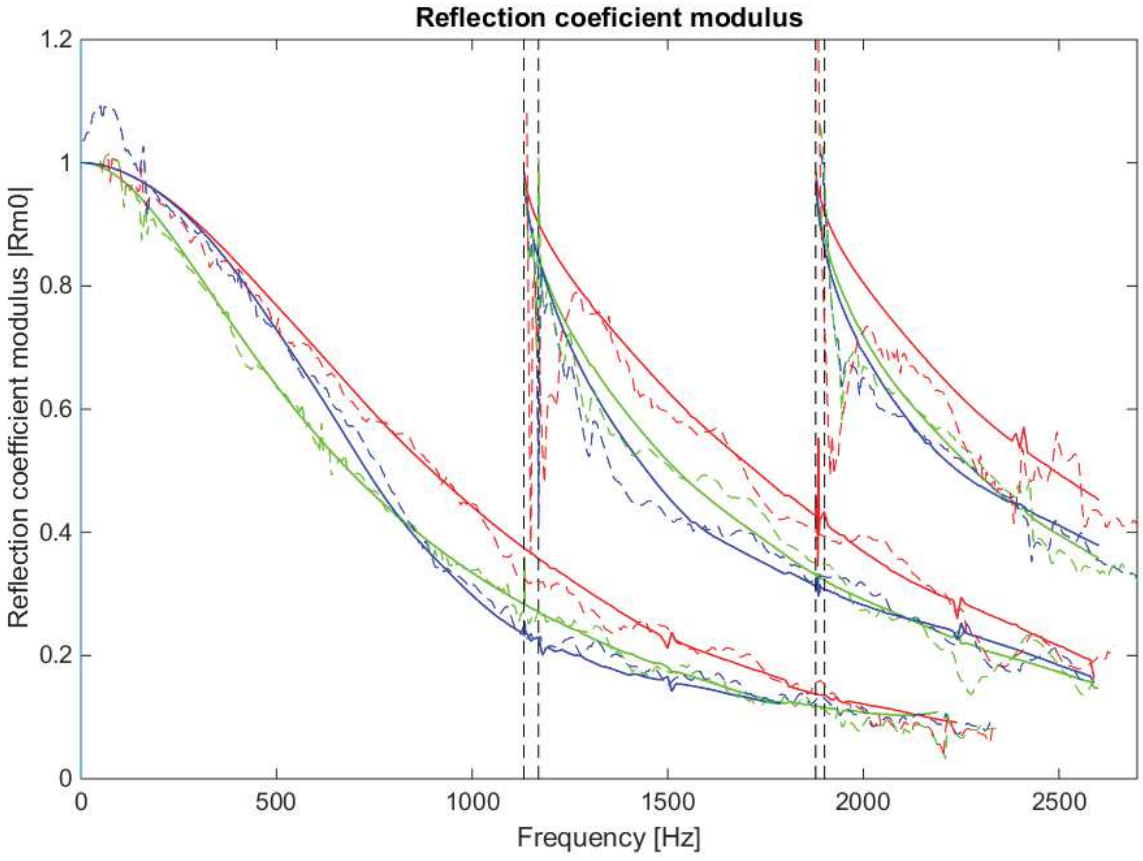

Figure 45 – Comparison of the reflection coefficient modulus results of numerical simulations (solid lines) and the experimental measurements (dashed lines), red curves correspond to the unbaffled pipe, green curves correspond to the baffled pipe and the blue ones correspond to the flanged pipe.

The numerical results and the measurements of the length correction are presented in figure 46. The comparison shows that numerical and the experimental curves are in a good agreement especially at frequencies far from the cut-off frequencies of the modes however there is a larger gap between the two results close to the cut-off frequencies. We can notice that all the curves of all configurations converge toward almost the same value $\delta/a \approx 0.25$ in high frequency range

$(f > 2000Hz)$.
Figure 47 gives more detailed plots of length correction curves for each mode.

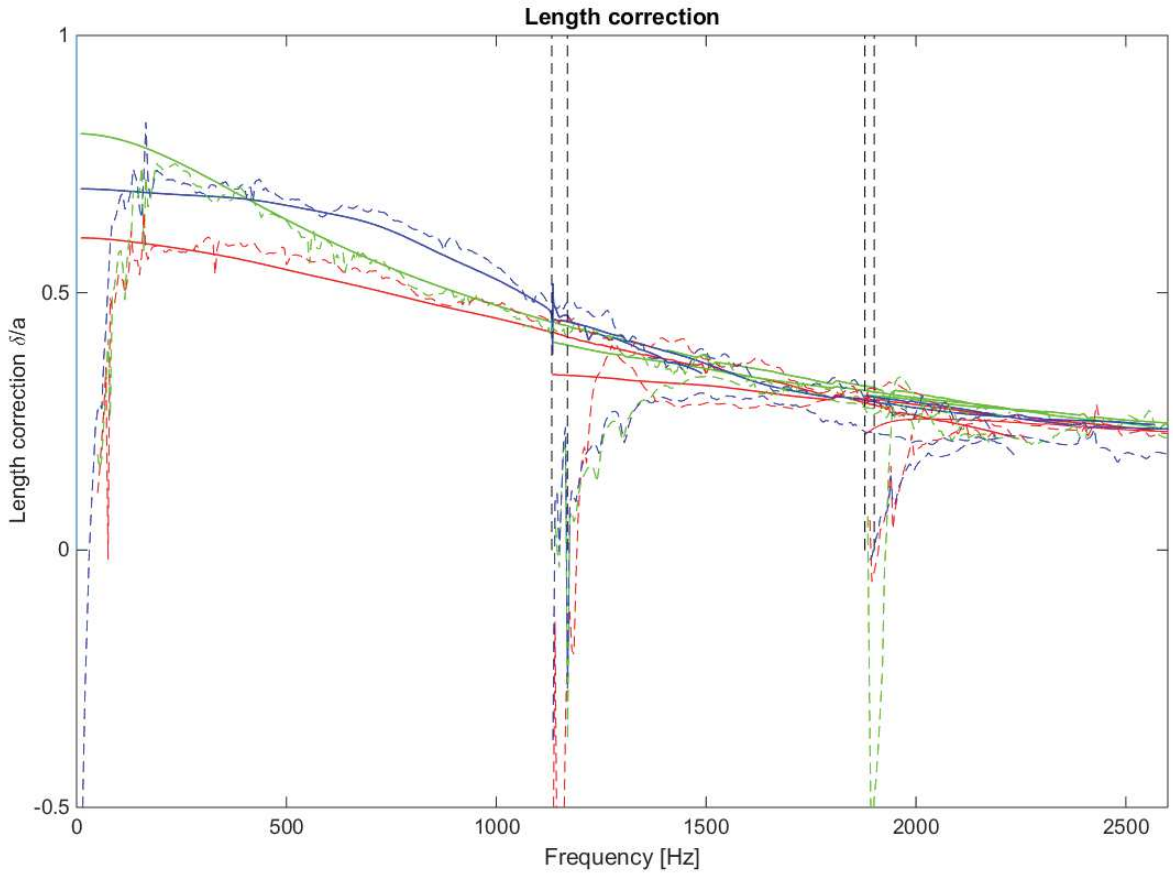

Figure 46 – Comparison of the length correction results, numerical simulations (solid lines), experimental measurements (dashed lines), red curves correspond to the unbaffled pipe, green curves correspond to the baffled pipe and the blue ones correspond to the flanged pipe.

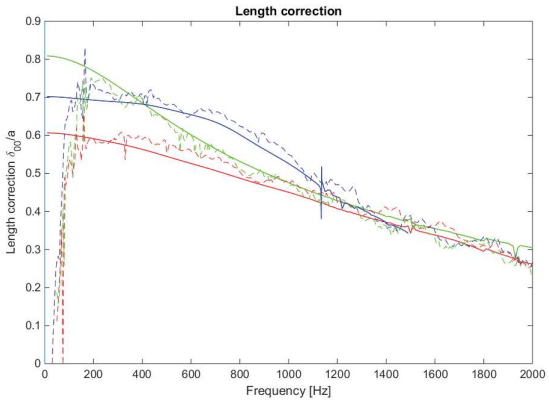

(a) Length correction for the plane mode (0.0).

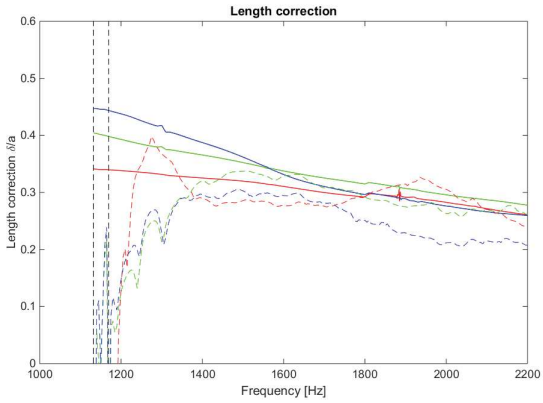

(b) Length correction for mode (1.0).

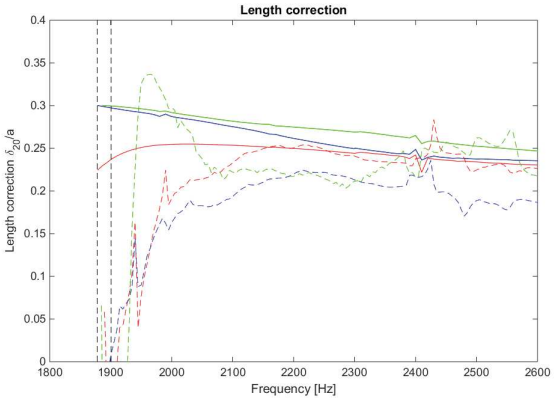

(c) Length correction for mode (2.0).

Figure 47 – Comparison of the length correction results, numerical simulations (solid lines), the experimental measurements (dashed lines), red curves correspond to the unbaffled pipe, green curves correspond to the baffled pipe and the blue ones correspond to the flanged pipe.

VI Conclusions:

In this study, numerical models are built in order to simulate the multimodal reflection phenomenon at the outlet of acoustic waveguides. Three models have been considered in order to cover almost all the possible and existing configurations in the industry: a pipe ended with an infinite baffle, a pipe ended with a finite flange and a pipe without a baffle.

The modal extraction is based on the method of measurement between microphone pairs, where the acoustic pressure is measured at two or more sections in order to calculate the unknown modal pressure amplitudes.

Sensitivity analysis represents a large part of this work, because testing the sensitivity of the numerical models to the simulation parameters is very important to evaluate the accuracy and the stability of the solutions. A large number of sensitivity calculation are performed not only on geometrical modal and its mesh but also on the post-processing codes to ensure that they represent exactly the numerical solution. Therefore additional codes are created just to test the post-processing codes using synthetic pressure signals and the conditioning proprieties of the matrices.

The comparison between the numerical results and the experimental measurements of Zhiping QIU [1] shows a good agreement between the simulations and the experiments. This comparison is very important for both the numerical and the experimental study especially for higher modes since the theoretical models are limited to the plane mode reflection.

For further studies, one can use more than two measurement sections in order to extract radial modes and avoid the interference between the decomposition of the azimuthal and radial mode as seen for the plane mode (0.0) and the first radial mode (0.1) in section V.1. Another option for the modal decomposition could be the control of the excitation to generate one mode at a time using an excitation that generates perfectly the signature of that mode.

References

[1] Zhiping QIU: Propagation en guide d'onde large: Mesures par antennerie microphonique de la réflexion multimodale pour différentes extrémitées, 2017

[2] Course by Dr.David Marx ENSIP: Propagation en guide, chapitre I, Equations sans dissipation.

[3] A.Snakowskaa, J. Jurkiewiczb and D. Smolikc: Open End Correction for Arbitrary Mode Propagating in a Cylindrical Acoustic Waveguide, ACTA PHYSICA POLONICA A, 2011

[4] Rayleigh 1896, The theory of sound, Chapter 16, Chapter 15 §302.

[5] Pierce 1989, Acoustics An Introduction to Its Physical Principles and Applications

[6] A.N. Norris and I.C. Sheng 1989 Journal of Sound and Vibration. 135, 85-93. Acoustic radiation from a circular pipe with an infinite flange.

[7] Mohamed Akoum, Jean-Michel Ville: Measurement of the reflection matrix of a discontinuity in a duct, 1998

[8] H. Boden and M. Abom : Influence of errors on the two-microphone method for measuring acoustic properties in ducts. Journal of the Acoustical Society of America 79(2), 541-549,1986

[9] H. Bailliet, R. boucheron, J. P. Dalmont, Ph. Herzog, S. Moreau, and J.C. Valiere: Setting up an experimental apparatus for the study of multimodal acoustic propagation with turbulent mean flow. Applied Acoustics 73, 191-197, 2012

[10] H. A. van der Vorst. Bi-CGSTAB: A fast and smoothly converging variant of Bi-CG for the solution of non symmetric linear systems. SIAM J. Sci. Stat. Comp., 13(2):631 644, 1992

[11] Comsol Multiphysics Users' Guide V4.3: 10 The Acoustics Branch, May 2012

[12] A. Bayliss, M. Gunzburger, and E. Turkel: Boundary Conditions for the Numerical Solution of Elliptic Equations in Exterior Regions. SIAM J. Appl. Math., vol. 42, no. 2, pp. 430-451, 1982.

[13] M. ABOM: Modal decomposition in ducts based on transfer function measurements between microphone pairs, KTH, 1989

Appendices

A Matlab programs:

Remark:

In this appendix only the important sections of each program are presented and the three dots (...) indicate that a part of the code is omitted.

Modal extraction code:

```
      (...)
Rmn=zeros(length(modes),length(f)); %Multimodal reflection matrix
PmnP=zeros(length(modes),length(f));%Modal pressure of the outgoing wave
PmnN=zeros(length(modes),length(f));%Modal pressure of the reflected wave
delta_mn=zeros(length(modes),length(f));%Length correction matrix
m=1;
while m<=length(modes)
     gamma_mn=(k.^2-(alpha_mn(m)/a)^2).^0.5; %Longitudinal wave-number
     Pmn_s=zeros(1,size(P0,2)); %Modal pressure at z=s
     Pmn_0=zeros(1,size(P0,2)); %Modal pressure at z=0
     mic=0;
     while mic <= N-1
        Pmn_s=Pmn_s+exp(-2j*pi*modes(m)*mic/N)*Ps(mic+1,:); % inv Fourier
        Pmn_0=Pmn_0+exp(-2j*pi*modes(m)*mic/N)*P0(mic+1,:);
        mic=mic+1;
     end
     Pmn_s=Pmn_s/N;
     Pmn_0=Pmn_0/N;
     %Calculation of the reflection coefficient and length correction:
     Rmn(m,:)=((Pmn_s-Pmn_0.*exp(-1j*gamma_mn*s))./
               (Pmn_0.*exp(1j*gamma_mn*s)-Pmn_s)).*exp(2j*gamma_mn*LB);
     delta_mn(m,:)=(angle(Rmn(m,:))-pi)./(-2*real(gamma_mn))+q*pi./real(gamma_mn);
     %Calculation of the modal pressure amplitudes:
     PmnP(m,:)=((Pmn_0-Pmn_s.*exp(-1j*gamma_mn*s))./(1-exp(-2j*gamma_mn*s)));
     PmnN(m,:)=((Pmn_0-Pmn_s.*exp(1j*gamma_mn*s))./(1-exp(2j*gamma_mn*s)));
     m=m+1;
end
      (...)
```

Read txt code:

```
      (...)
file = fopen(char(link)); %Open the Pressure data file
      (...)
lineSplit=strsplit(line); %Read the frequency line
freq=[];
for fi=lineSplit(5:end-1)                    %Load the frequency line
    freqi=str2double(strsplit(char(fi),'='));%Convert from str to double
    freq=[freq freqi(2)];                    %Save the value in frequency vector
end
      (...)
P_0=[];     %Pressure measured at z=0
P_s=[];     %Pressure measured at z=s
X_0=[];     %Coordinates of the probes at z=0
X_s=[];     %Coordinates of the probes at z=s
while ischar(line)
    lineSplit=str2double(strsplit(line));%Load a line
    if lineSplit(3)==zmic0               %Check it it's a probe
        P_0=[P_0 ; lineSplit(4:end-1)]; %Save the pressure in the pressure vector
        X_0=[X_0 ; real(lineSplit(1:3))];%Save the coordinates of the probe
    end
    if lineSplit(3)==zmics
        P_s=[P_s ; lineSplit(4:end-1)];
        X_s=[X_s ; real(lineSplit(1:3))];
    end
    line = fgetl(file);                  %Go to the next line
end
  fclose(file);      %Close the file
  ii=1;
  Pxz0=[];      %Average pressure over 3 neighboring probes at z=0
  Pxzs=[];      %Average pressure over 3 neighboring probes at z=s
  X0=[];        %Coordinates of the probes at z=0
  Xs=[];        %Coordinates of the probes at z=s
  while ii<= size(P_0,1)-2    %Calculate the average pressure
                              %over each 3 neighboring probes
      Pxz0=[Pxz0 ;(P_0(ii,:)+P_0(ii+1,:)+P_0(ii+2,:))./3];
      Pxzs=[Pxzs ; (P_s(ii,:)+P_s(ii+1,:)+P_s(ii+2,:))./3];
      X0=[X0 ; (X_0(ii,:)+X_0(ii+1,:)+X_0(ii+2,:))./3];
      Xs=[Xs ; (X_s(ii,:)+X_s(ii+1,:)+X_s(ii+2,:))./3];
      ii=ii+3;
  end
      (...)
```

Pressure signal test:

```
  (...)
k=2*pi*f/c0; %Total wave-number
gamma_mn=(k.^2-(alpha_mn(2)/a)^2).^0.5;  %Axial wave-number
cutindix=find(f>=1132,1); %Find the cut-off frequency index
C10=[zeros(1,cutindix-1) ones(1,length(f)-cutindix+1)]; %Max Pessure amplitude
Jm=besselj(1,alpha_mn(2));                              %Bessel func
Pmic_0=[];    %Pressure vector at the first section
Pmic_s=[];    %Pressure vector at the second section
delta=a./(1+f.^2);    %Length correction function
Rs=-3*[zeros(1,cutindix-1)
       ones(1,length(f)-cutindix+1)];%|R| at the reflection pt
R=Rs.*exp(-2j*gamma_mn.*(LB+delta)); %|R| at the first section
  (...)
while ii<=8  % Pressure at the first section
    Pmic_0=[Pmic_0 ; C10.*(1+R).*exp(1j*m*ii*tetha)];
    ii=ii+1;
end
  (...)
while ii<=8  % Pressure at the second section
    Pmic_s=[Pmic_s ; C10.*(exp(-1j*gamma_mn*s)+
             R.*exp(1j*gamma_mn*s))*exp(1j*m*ii*tetha)];
    ii=ii+1;
end
  (...)
```

B Control of the excitation using 16 loudspeakers:

In theory, if the excitation generates perfectly the signature of only one mode only that mode could propagate in the wave guide. The modal signature are continuous functions (see equation 16) so theoretically the modal signature must be generated using a continuous source. Unfortunately it's impossible to build such source in Comsol Multiphisics environment, the reason why we limited our source to a 16 loudspeakers placed on the circumference of the pipe. The loudspeakers are modeled with half pulsating spheres on the circumference of the pipe (half of a sphere in a baffle). Using discrete 16 loudspeakers doesn't generate perfectly the modal signature however it allows to have only one dominant mode. The loudspeakers are controlled to generate the first higher mode (1.0) using equation 16. Figure 48 shows how the loudspeakers are controlled.

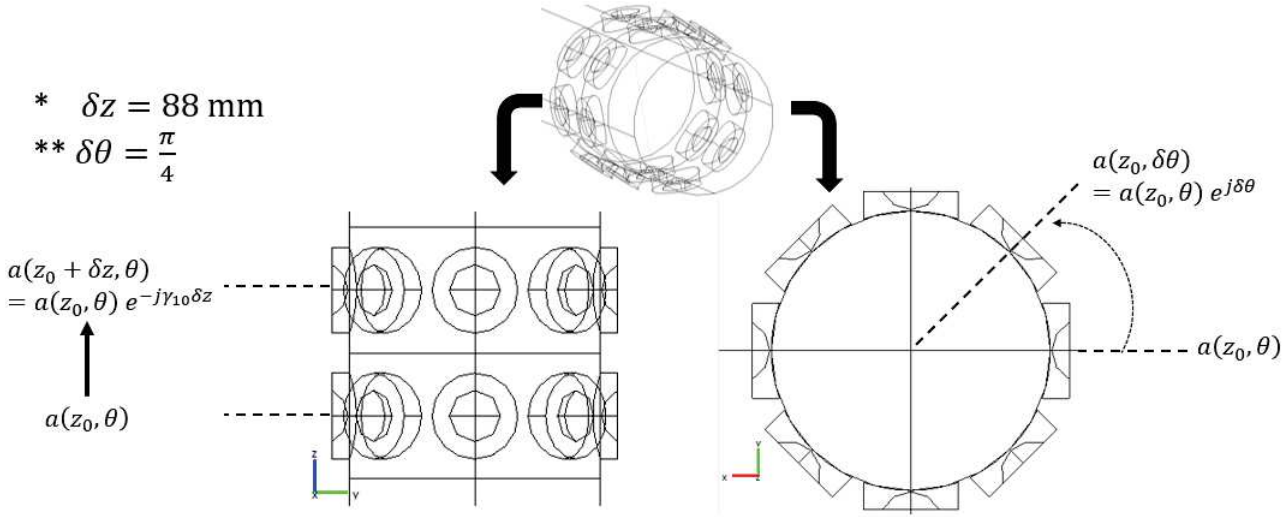

Figure 48 – Control of the loudspeakers to generate the first higher mode (1.0).

Figure 49 shows the total pressure field before the modal decomposition. The results using only 16 loudspeakers are relatively satisfying compared to the results obtained with only one loudspeaker however we noticed that at some frequencies we still have an interaction with other modes. We can also notice that the spiral of the longitudinal propagation of the mode is more visible.

Figure 50 compares the modal pressure amplitude of the plane mode and mode (1.0) using one loudspeaker and 16 loudspeakers. According to figure 50 (a) modal amplitude of the plane mode is about 0.1pa and the amplitude of mode (1.0) is about 400pa which confirms that mode (1.0) is dominating. Contrary in figure 50 (b) we can notice that the two modes have almost the same amplitude.

In conclusion using multiple discrete sources allow to propagate one dominant mode however it's not possible to eliminate completely the other modes which requires a continuous source.

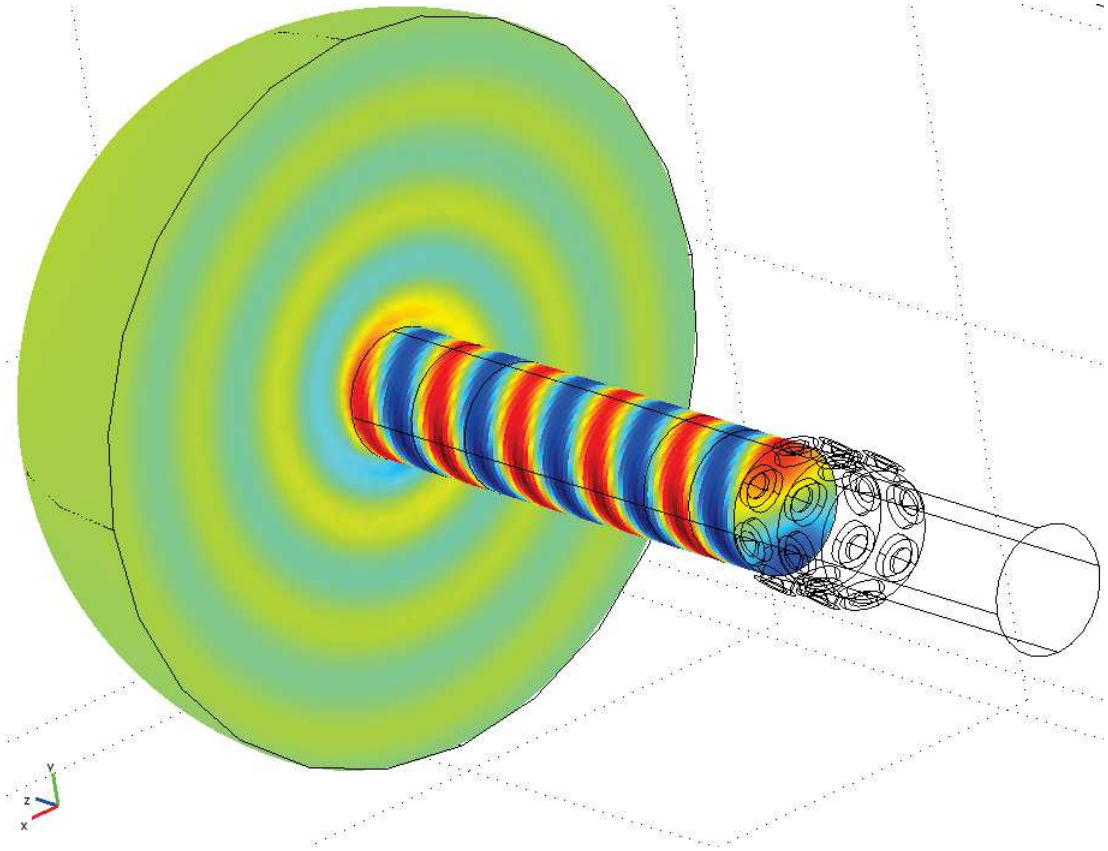

Figure 49 – Total pressure field generated with 16 loudspeakers set to mode (1.0).

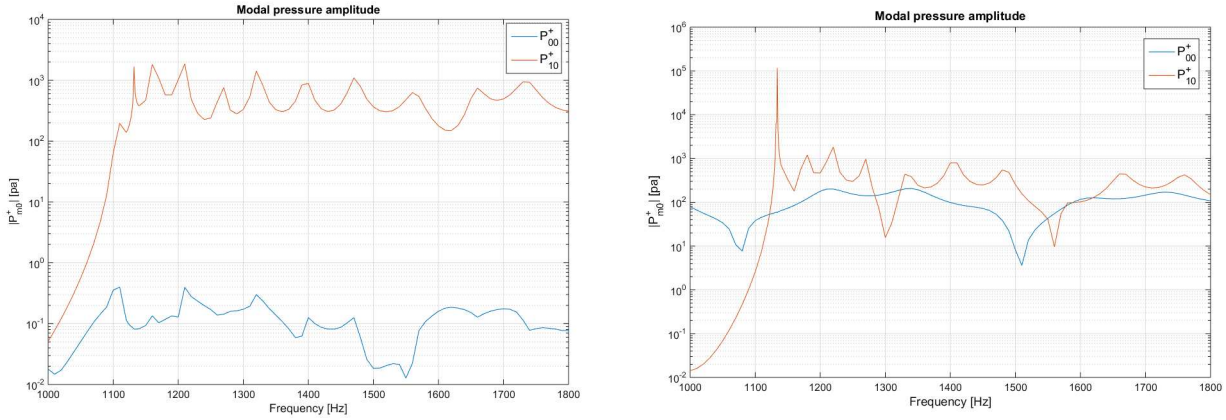

(a) Using 16 loudspeakers.

(b) Using only one loudspeaker.

Figure 50 – Comparison of the modal pressure amplitude of modes (0.0) and (1.0) obtained with different excitation.